Master's thesis
Meteorology

Slope and valley winds in the Himalayas as simulated by the Weather Research and Forecasting model

Johannes Mikkola

November 17, 2020

Supervisor: Docent Victoria Sinclair

Examiners: Professor Heikki Järvinen
                 Docent Victoria Sinclair

HELSINGIN YLIOPISTO — HELSINGFORS UNIVERSITET — UNIVERSITY OF HELSINKI

Tiedekunta — Fakultet — Faculty	Koulutusohjelma — Utbildningsprogram — Education programme
Faculty of Science	Master's Programme in Atmospheric Sciences

Tekijä — Författare — Author
Johannes Mikkola

Työn nimi — Arbetets titel — Title
Slope and valley winds in the Himalayas as simulated by the Weather Research and Forecasting model

Opintosuunta — Studieinriktning — Study track
Meteorology

Työn laji — Arbetets art — Level	Aika — Datum — Month and year	Sivumäärä — Sidoantal — Number of pages
Master's thesis	November 17, 2020	63 pages

Tiivistelmä — Referat — Abstract

Local mountain winds have a diurnal cycle of flowing up the slopes and valleys daytime and down nighttime. It is important to improve the understanding on these thermally driven winds, because they have a major role in pollution transport in mountain areas, which are highly sensitive for air-quality problems. This thesis determines if the slope and valley winds in the Khumbu valley, Himalayas, are driven by the textbook mechanisms.

By the textbook mechanisms the slope and valley winds are driven by horizontal temperature differences caused by uneven heating over an area of complex terrain. Slope winds are driven by the horizontal air temperature difference in the slope surface vicinity when the slope surface is heated or cooled. Valley winds are driven by the uneven heating caused by the air volume difference between the valley and above an adjacent plain. If the valley slopes narrow and the floor is elevated towards the head of the valley, both the valley and slope wind mechanisms drive the winds along the valley.

The slope and valley winds in the Himalayas are studied using Weather Research and Forecasting model (WRF), that is run for 5 days period in December 2014 with 1 kilometer horizontal grid spacing and 61 vertical levels. Earlier studies have shown that WRF is capable of simulating the thermally driven mountain winds on this resolution with the length scales of the Khumbu valley topography.

Horizontal gradient of air temperature and slope wind component at the slope surface have a matching daily cycle in the lower and middle parts of the valley. The boundary layer air volume decreases from the mouth of the valley towards the middle parts of the valley indicating the valley wind mechnanism. The daytime potential temperature profiles yield that also the slope wind mechanism drives the winds along the valley.

The slope winds have a textbook daily cycle in the lower and middle parts of the valley and the analysis yields that they are driven by the slope wind mechanism. In the upper part of the valley the thermally driven slope winds are dominated by synoptic scale channelling and gravity wave developing into the valley. The daytime up-valley winds are driven by both valley wind mechanism and slope wind mechanism due to the valley narrowing and elevation towards the head of the valley, respectively. Nocturnal along-valley winds are weak less than 0.5 meters per second flowing up or down-valley. The wind patterns are similar to what is shown in earlier studies done in Khumbu valley.

Avainsanat — Nyckelord — Keywords
mountain meteorology, slope wind, valley wind, WRF, Khumbu valley

Säilytyspaikka — Förvaringsställe — Where deposited
HELDA - Digital Repository of the University of Helsinki

Muita tietoja — övriga uppgifter — Additional information

Contents

1. Introduction

Mountain orography creates an interesting wind system with daily developing mountain winds. These thermally driven local winds play an important role in the transport of pollution in the mountain areas. The vertical transport of aerosol can be up to 3.5 times higher in the mountains compared to over flat terrain (Wagner et al., 2015a). Due to strong inversion layers and regional winds flowing day-to-day along the same paths, valleys and basins are also highly sensitive for severe air-quality problems (Whiteman (2000), Diémoz et al. (2019), Gohm et al. (2009)). Now considering that one third of Earth land surface is covered by mountains, just by the definition of orography elevation, the local circulation in mountains deserves more detailed research (Rotach et al., 2014).

The thermally driven mountain winds concentrated in this thesis are slope and along-valley winds that flow along the slopes and valley-axis, respectively. By textbook theory, the slope winds are driven by horizontal temperature differences caused by the slope heating and cooling by solar radiation and outgoing longwave radiation, respectively (Whiteman (2000), Markowski and Richardson (2010)). The air in the vicinity of the surface is warmed and cooled by the surface creating a temperature difference between the air at the same height out from the slope which results in an imbalance of gravity and buoyancy. The along-valley winds instead are driven by the differential heating and cooling caused by the difference in air volume for the same horizontal area above a valley and an adjacent plain. Given the same

rate of solar heating or longwave radiative cooling, the smaller air volume between the slope walls results in greater temperature changes compared to the air above the adjacent plain. The aim of this thesis is to determine if the slope and along-valley winds in the Himalayas are driven by textbook mechanisms.

The analysis of this study concentrates on the local mountain winds in Khumbu valley, which is one major valley in the Nepal Himalayas leading to the base of Mount Everest. The steep inclination towards the Mount Everest and Tibetian Plateau affects both the thermally driven winds and the variability of climates along the valley (Karki et al., 2016). The climates vary from the low elevations sub-tropics to the Mount Everest base polar tundra just within less than 100 kilometers. Wagner et al. (2015b) found in their idealised valley simulations with heterogeneous along-valley geometry enhanced along-valley winds due to the valley elevation and narrowing towards the head of the valley, which makes the Khumbu valley an interesting area to examine the role of the textbook theories of the mountain winds.

The slope and valley winds in Khumbu valley are studied using a high resolution simulation performed with the Weather Research and Forecasting model (WRF). In earlier studies WRF has been shown to be capable of simulating the local mountain winds when run with 1 kilometer horizontal resolution (Giovannini et al. (2014a), Potter et al. (2018)). The simulation used in this study is compared with the other studies considering the local winds in the Khumbu valley. The characteristics of the slope and valley winds are similar compared to studies with modelling (Potter et al., 2018) and observations (Bollasina et al. (2002), Shea et al. (2015)).

2. Theory and background

2.1 Atmospheric boundary layer

The atmospheric boundary layer (ABL) is defined as the part of the troposphere which is in direct interaction with the Earth surface (Holton and Hakim, 2013). The flow field in ABL responds to surface forcing within a timescale of an hour or less (Stull, 1988). Flow conditions in the ABL are highly dominated by shear-induced turbulent eddies and fluxes between the atmosphere and the surface. Although molecular viscosity is significant only in the closest millimeters to the surface it affects the whole ABL by taking wind velocity to zero just in the vicinity of the surface (Holton and Hakim, 2013). In this way even the smallest wind speeds create wind shear which combined with buoyancy results in turbulent eddies that transport heat, momentum and energy fluxes between Earth surface and the atmosphere. In the mountain areas, ABL is the part of the atmosphere where the thermally driven slope and along-valley winds occur.

The turbulent eddies in ABL act on length scales from viscous sublayer (10^{-3} meters) to boundary layer depth (10^3 meters). The boundary layer depth varies from only tens of meters up to three kilometers depending on the climate, weather and time of the day. In free troposphere (FT) the turbulent motions and viscosity does not dominate the flow conditions and the diurnal cycle of wind field or temperature are insignificant (Stull, 1988).

The diurnal cycle of ABL consists of four main stages: evening transition period, nocturnal decoupled period, morning transition period and daytime coupled period (Whiteman, 2000). The diurnal cycle of ABL vertical structure is illustrated in Figure 2.1. After sunrise the turbulent heat flux starts to warm the boundary layer. This convective turbulence destroys the stable layer formed during the night. Eventually the convective boundary layer (CBL) may become well mixed between the surface layer and entrainment zone (EZ) meaning the potential temperature and wind profiles are nearly constant throughout the ABL (Holton and Hakim, 2013). The entrainment zone refers to the layer separating CBL and FT. Exchange processes between ABL and FT take place in EZ, such as vertical transport of pollution between the layers or tropospheric air entrainment into ABL (Foken, 2008). Daytime period is termed coupled because the ABL and FT are coupled through EZ, whereas ABL and FT are separated by inversion layer during nocturnal decoupled period (Whiteman, 2000). Morning transition period starts when solar radiative heating exceeds outgoing longwave radiative cooling and vice versa for evening transition period.
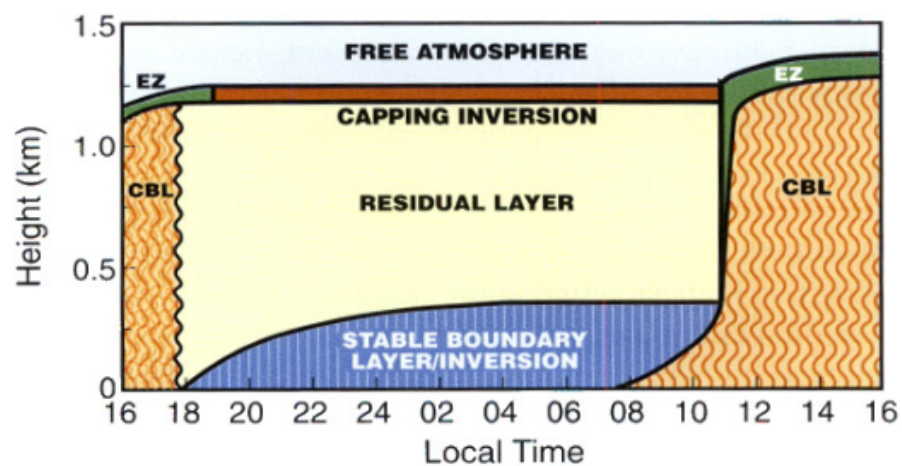

Figure 2.1: Schematic diurnal cycle of boundary layer structure over a flat terrain. CBL and EZ stand for convective boundary layer and entrainment zone, respectively. Adapted from Whiteman (2000), Figure 4.14.

In cold climates or in cloudy weather the stable layer may stay prominent if the surface heating is weak. The nocturnal boundary layer is characterised by a stable layer growing from the surface and weaker turbulent flows. Above the stable layer lays a so-called residual layer, which are remains of the mixed turbulent layer.

2.1.1 Atmospheric boundary layer over mountain terrain

The boundary layer over mountains is divided in mountain, slope and valley atmospheres (Ekhart, 1948), which is illustrated in Figure 2.2. Slope and valley atmospheres are characterised by thermally driven slope, valley and cross-valley winds (Whiteman, 2000). These local winds flow up slope and valley surfaces daytime and down nighttime. Compensatory flows blow the opposite dircetion in closed circulation aloft within the valley atmosphere. Mountain-plain winds flow in the mountain atmosphere with similar pattern but in a larger scale circulation. The diurnal cycle or parts of it may be dominated by local topography induced or strong synoptic scale flows. The thermally driven local winds are described in details in Section 2.2.
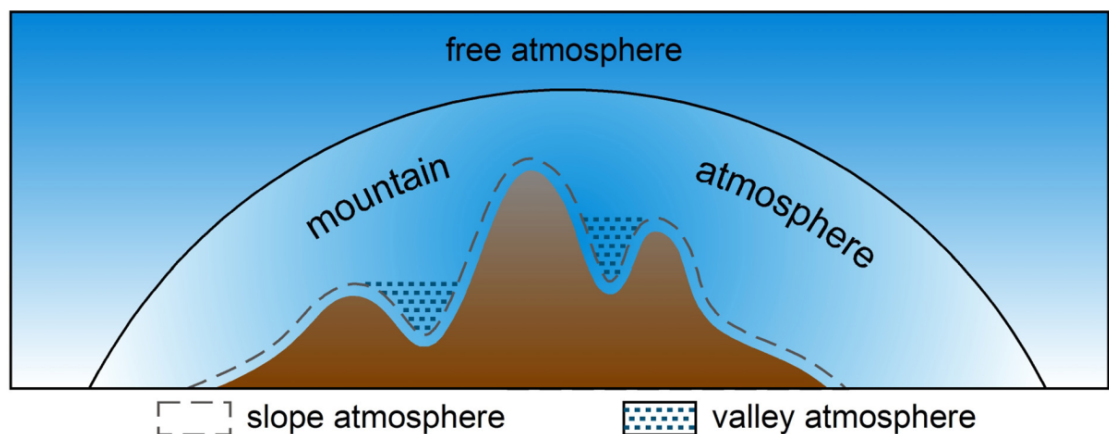
Figure 2.2: Dashed line and hashed fill indicate slope atmosphere and valley atmosphere, respectively. Boundary between free troposphere and atmosphere influenced by mountain marked with solid line. Adapted from de Wekker and Kossmann (2015), Figure 1.

The boundary layer in slope and valley atmosphere differs from one over flat terrain. Since the terrain is horizontally heterogeneous, the vertical structure of boundary layer differs over the slopes and valley center (Whiteman, 2000).

The evening transition period starts slightly before sunset when the longwave radiative cooling exceeds the surface heating by the solar radiation (Figure 2.3a–b). Cool air flows down the slopes which creates a cold pool that grows in height from the valley bottom. On top of the cold pool there is a residual layer which is characterised by up-valley winds (Figure 2.3c) (de Wekker and Kossmann, 2015). The evening transition period ends when the residual layer is ceased or the cold pool fills the entire valley atmosphere and the down-valley winds blow through the depth of the valley (Whiteman, 2000).

The nocturnal phase is called decoupled for two reasons (Whiteman, 2000). The inversion at ridge height prevents air exchange between the valley and FT. Also the ridges protect the flows within the slope and valley atmospheres from large scale flows aloft the valley. The depth of the cold pool depends on the surface cooling rate compared to climate and ridge line height, the inversion layer may exceed above the ridges or stay within the valley.

The morning transition period starts right after sunrise, when the surface heating by solar radiation exceeds the longwave radiative cooling. The stable core is destroyed from above by the descending flow that is caused by the convergence of cross-valley circulation at the crest height above the center of the valley (Figure 2.3d–e) and from below by the mixed layer. The cross-valley circulation pointed towards the center of the valley at the crest height originates from the up-slope winds blocked by capping inversion (Catalano and Cenedese, 2010). The mixed layer stays moderate shallow, compared to one over a flat terrain, because the slope flows take air out from the valley floor (Stull, 1988). The stable core is destroyed in

three to five hours after sunrise (Whiteman and McKee, 1982) ending the morning transition phase.

The daytime coupled period refers to a fully developed CBL extending above the ridge height (Figure 2.3f). The valley atmosphere is then coupled to the free atmosphere above ridges and the large-scale flows channel easier to dominate the thermally driven flows (de Wekker and Kossmann, 2015). Depending on the valley depth and local topography the slope wind circulation may have multiple cells separated by inversion layers within the valley during the coupled period (Wagner et al., 2014). Wind speeds reach their maxima in the afternoon and wind direction turns katabatic before sunset when the evening transition period starts again (Whiteman, 2000).
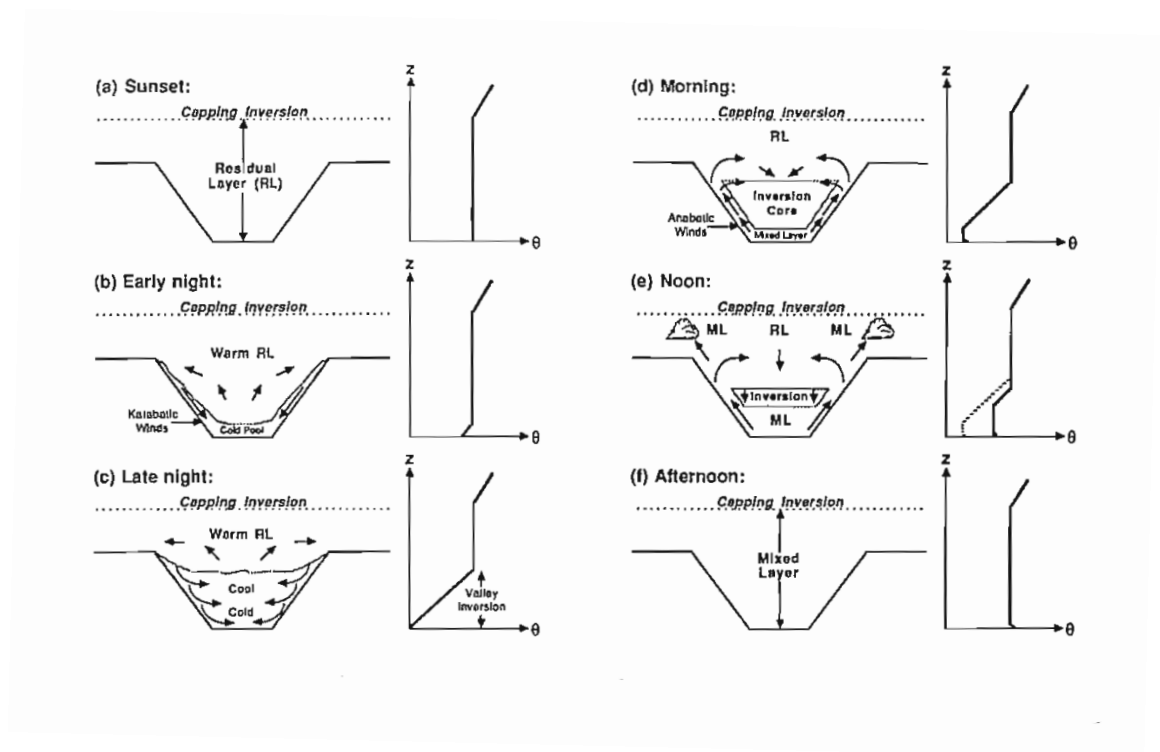
Figure 2.3: Idealised diurnal cycle of cross-valley circulations and layers with different static stabilities in a valley atmosphere. RL and ML refer to residual and mixed layer, respectively. Adapted from Stull (1988), Figure 14.2.

2.2   Diurnal mountain winds

Diurnal mountain winds consist of four major components: slope winds, along-valley winds, mountain-plain winds and cross-valley winds (Whiteman, 2000). Briefly, the winds blow up-slope, up-valley and from plain to mountain during daytime and down-slope, down-valley and from mountain to plain during nighttime. Often the different wind components can be difficult to separate from each others because their cycles overlap and magnitudes differ locally. Usually the wind direction at slope surface circles from morning up-slope to afternoon up-valley and in evening transition period from down-slope to nocturnal down-valley winds. Complex terrain causes local differences in wind magnitudes due to differential shading or other varying surface properties like albedo and latent heat. These mountain winds are driven by horizontal temperature differences caused by uneven warming and cooling and they are strongest on days with clear sky and weak synoptic scale wind. As the aim of this thesis is to determine if typical textbook driving mechamisms for mountain winds apply in the Himalayas, these driving mechanisms for slope, valley and cross-valley wind components are described in the following Sections 2.2.1, 2.2.2 and 2.2.3, respectively.

Most of the theories considering mountain winds have been developed based on observations or idealised modelling simulations. Majority of the observation campaigns are done in European Alps or Rocky Mountains in Northern America. The advantage of idealised simulations is to get clearer view of the thermally driven phenomena in a highly controlled simulation environment. The idealisations mean for example a use of simplified valley topographies or absence of large scale weather forcing.

Various studies in the past decades have evaluated the capability of numerical weather prediction models capturing the thermally driven mountain winds (Giovannini et al. (2014b), Giovannini et al. (2014a), Giovannini et al. (2017), De Wekker and

Fast (2005), Rotach and Zardi (2007)). The common conclusion from these studies is that the weather models are eligible to simulate the thermally driven valley winds with 1 kilometers resolution. Models used in aforementioned studies were Weather Research and Forecasting model, WRF (Giovannini et al. (2014a), Giovannini et al. (2014b)), Consortium for Small-Scale Modelling Model, COSMO (Schmidli et al. (2018)) and Regional Atmospheric Modelling System, RAMS (De Wekker and Fast (2005)). RAMS had troubles in simulating the onset of up-valley winds ending up in 2 hours delay in the morning transition period which was caused by the inability to model shading effect of surrounding topograpy around the sunset and sunrise. COSMO was able to resolve the valley winds in large and medium sized valleys. Schmidli et al. (2018) found also a requirement of high resolution surface topography and land use data for capturing the valley wind magnitudes well. Capability of WRF is described in details in Section 3.2.
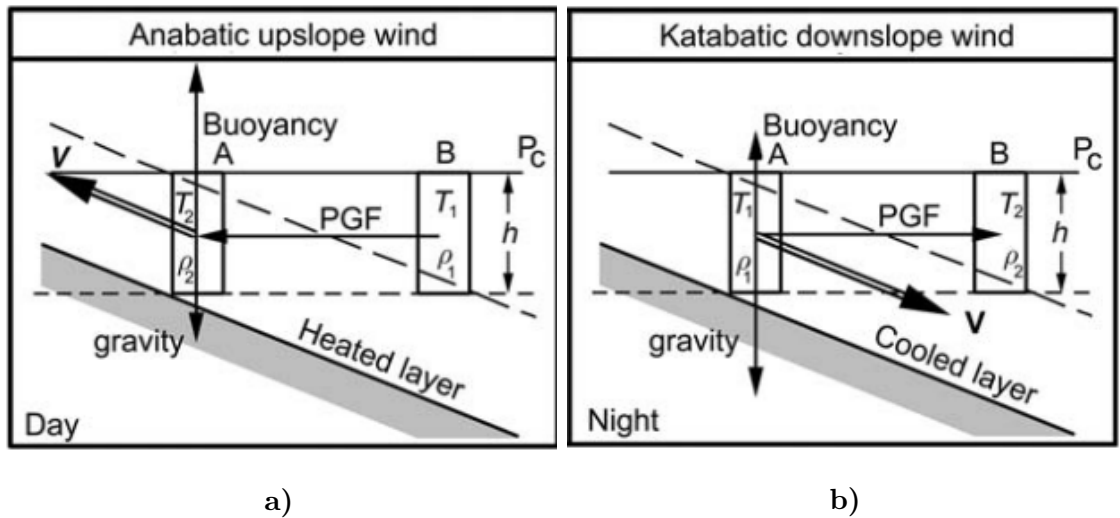
2.2.1 Slope winds

Slope winds are driven by horizontal temperature difference in air adjacent to the slope surface (Markowski and Richardson, 2010). During daytime the slope surface is heated by solar radiation which leads to air being warmer close to the surface than away from it on the same height which is illustrated in the Figure 2.4a, where the horizontal isentropes are pointed downwards in the vicinity of the surface. Potentially warmer air accelerates upwards when bouyancy force acts stronger than gravity in the air parcel at the surface (Figure 2.5a). Pressure gradient force caused by the warmed air keeps the flow towards the slope (Stull, 2011), which is marked with PGF in Figure 2.5a. The same process happening along the slope at each height produces an up-slope blowing wind layer. The simple model for daytime up-slope wind circulation is illustrated in Figure 2.6a, where slope winds blow in the

CBL and towards the valley center above CBL, with corresponding descending flow above the valley center (de Wekker and Kossmann, 2015).
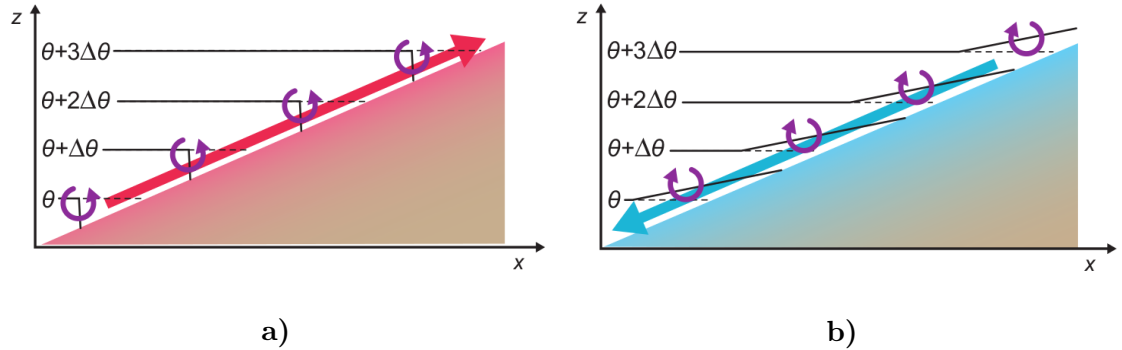
Figure 2.4: Potential temperature (θ) profiles that develope a) daytime up-slope winds and b) nighttime down-slope winds. Adapted from Markowski and Richardson (2010), Figure 11.1.

Figure 2.5: Force diagram in the process of a) up-slope winds and b) down-slope winds. Vectors V and PGF denotes wind vector and pressure gradient force, respectively. In this figure $T_1 < T_2$ and $\rho_1 > \rho_2$. Adapted from Barry (2008), Figure 3.32.

Aforementioned slope wind process happens reversed when longwave radiation is cooling the slope surface during nighttime and the down-slope winds blow along the slope. For downslope winds at the surface the isentropes point upwards in the vicinity of surface (Figure 2.4b) and the gravity force exceeds buoyancy (Figure

2.5b). The driving mechanism acts the strongest in early hours of the transitions periods (Whiteman, 2000) when the temperature gradients are at the strongest.

The magnitude of slope winds is around 1–5 meters per second and the depth of the up-slope (down-slope) winds varies from 50 to 150 (10 to 40) meters after the transition period (Whiteman, 2000). Despite that the horizontal temperature gradients are the strongest near the surface, the slope wind maxima is typically found in up-slope and down-slope winds on heights 10–20 meters and 1–3 meters above the surface, respectively. Aforementioned surface friction reduces the wind speed in the surface vicinity. The depth of the up-slope wind layer increases with increased elevation (Markowski and Richardson, 2010). With increasing depth also volume flux increases as there is air entrained from the upper boundary of the slope wind layer (Zardi and Whiteman, 2013).

The classical slope wind circulation in Figure 2.6a is typically found in wide or low valleys (Rotach et al., 2015). With strong capping inversion below crest height, the slope wind circulation can be limited in lower heights (Figure 2.6c)(de Wekker and Kossmann, 2015). During the coupled period when the CBL has grown height from the valley bottom the returning circulation occurs within the CBL and is mixed with the up-slope winds (Figure 2.6d). In this stage the up-slope winds get weaker or absent.

Up-slope winds act most pronounced with aforementioned clear sky, weak to moderate ambient wind but also in an initially stable valley atmosphere. Different cloud types absorb and reflect longwave and shortwave radiation differently but overall the slope wind circulation is stronger with clear sky. Ohata et al. (1981) found the thermally driven local winds to decrease in magnitude almost by a third when Khumbu valley was coveraged by clouds in the Himalayas. In an unstable valley atmosphere the up-slope wind layer would not be observed, since the convec-
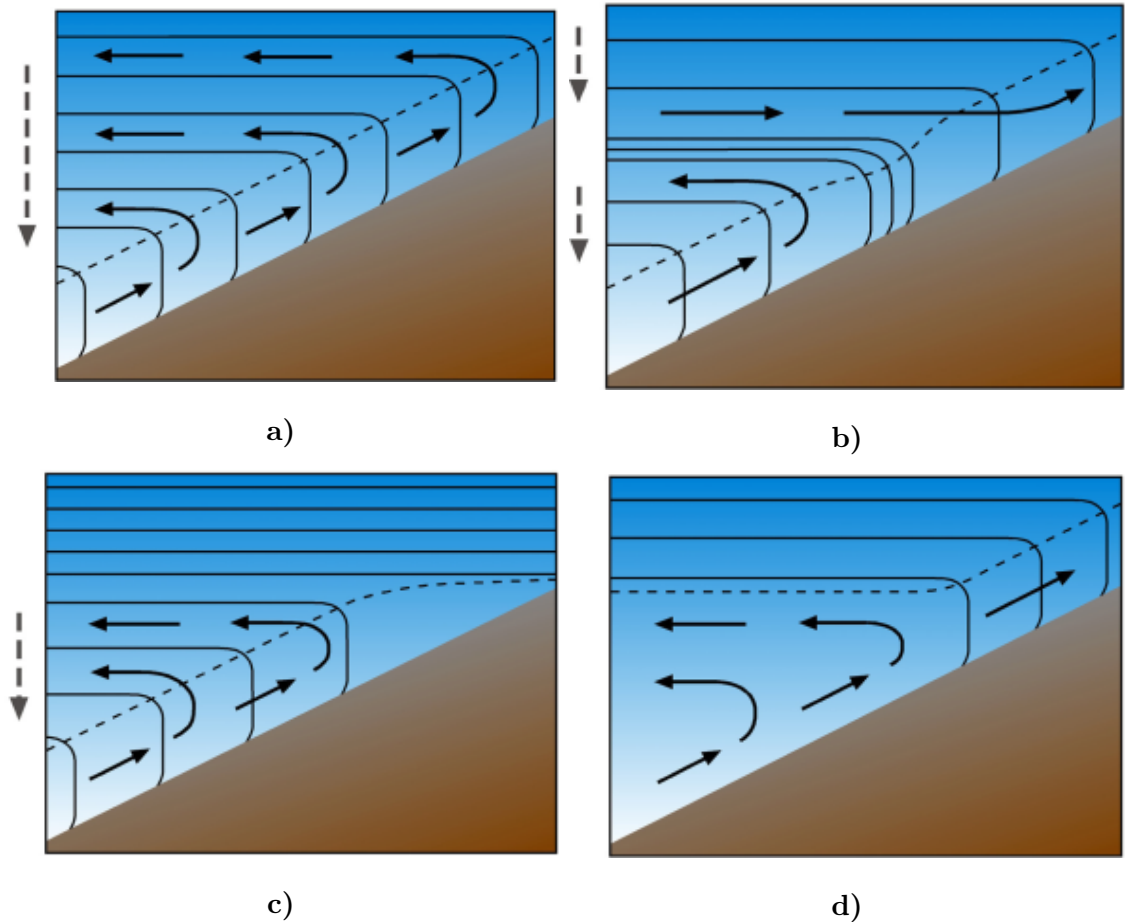
Figure 2.6: Conceptual models of daytime up-slope wind circulations and CBL height over heated slope. Solid and dashed lines denote isentropes and CBL height, respectively. Solid and dashed arrows denote air flow over the slope and corresponding subsidence flow over the center of the valley. Adapted from de Wekker and Kossmann (2015), Figure 4.

tion would raise air parcels vertically, instead of developing the up-slope wind layer (Orville, 1964).

In the northern hemisphere, south facing slopes have the strongest up-slope winds and north facing slopes the weakest (Barry, 2008). The difference in up-slope winds between south and north facing slopes is significant, for example in the Inn valley in Austria that is east-west orientated (Gohm et al., 2009). The slope wind cycle between east and west facing slopes are slightly delayed from each other as

the west slope is sun lit earlier in the morning and east slope later in the evening (Barry, 2008).

For slopes with varying slope angle (Barry, 2008) and surface properties the slope wind velocities vary along the slope (Whiteman, 2000). Increased soil moisture and surface albedo would weaken the driving mechanism for up-slope winds due to decrease in sensible heat flux and absorbed sun radiation. Gohm et al. (2009) found a layered flow separation of up-slope winds towards the valley center caused by changes in the slope angle and surface albedo along the Inn valley. Ohata et al. (1981) found the thermally driven winds to decrease in magnitude when Khumbu valley were covered in snow. For uniform slope angle the down-slope winds would have the down-slope maximum near the base of the slope (Barry, 2008). In concave shaped valleys the maximum is found in the steepest part and lower wind speeds in the base.

2.2.2   Along-valley winds

The magnitude of the valley wind maxima is 3–10 meters per second and is typically found at height 30–60% of the inversion layer height (Whiteman, 2000). The strongest down-valley winds are usually found at the mouth of valley, in the so-called valley exit jet. Near the valley exit the valley-plain pressure gradient is the strongest, caused by abrupt change of topography. Cold air sinking along the valley also causes the down-valley wind velocities to increase with distance. In valleys without major constrictions along the valley axis, the valley wind layer increases both in depth and wind speed with distance which means an increase in mass flux (Zardi and Whiteman, 2013). Returning circulation for valley winds are sometimes observed below ridge height, in the stable core or residual layer (Whiteman, 2000). The returning wind is usually weaker and often not observed.
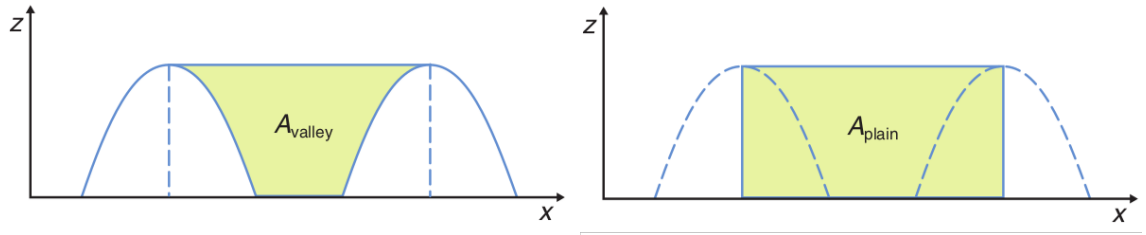
Figure 2.7: Cross sections of air for equal horizontal length taken across a valley and above a plain. Adapted from Markowski and Richardson (2010), figure 11.9.

The main driving mechanism for diurnal along-valley winds are temperature gradients between the valley atmosphere and air above the adjacent plain (Markowski and Richardson, 2010). Taken an equal cross section of atmosphere across the valley and above a plain, the air volume in the valley is smaller than above the plain (Figure 2.7). From the first law of thermodynamics, one can say that for equal heating the air in the valley will warm faster. This causes a pressure gradient force pointing towards the valley and results in a daytime up-valley wind. The same process is reversed with longwave radiative cooling nighttime, causing the air in the valley to cool down faster than the air above the plain. Now the pressure gradient force points down the valley towards the plain and it drives the nocturnal down-valley winds. For along-valley winds to form it is not necessary for the valley floor to be elevated along the valley-axis. If the valley floor is sloped the slope wind mechanism, described in previous section 2.2.1, will act also along the valley. Synoptic-scale pressure gradients can also cause along-valley winds that do not have a diurnal cycle (Zardi and Whiteman, 2013). Pressure-driven channeling drives wind along the valley-axis from higher to lower pressures.

The effects of valley geometry and along-valley axis heterogeneity was studied using idealised valley simulations by Wagner et al. (2015a) and Wagner et al. (2015b). Tilting the valley floor and narrowing the valley towards the head of the valley caused a major increase in the up-valley wind speeds. When the valley air volume was reduced by half, the up-valley wind speeds doubled and up-valley winds

were found to penetrate further up the valley with both tilted valley floor and narrowing slopes (Wagner et al., 2015a). Constrictions and local height minima along valley-axis cause cold pools with night-time down-valley winds (Whiteman, 2000).

Rampanelli et al. (2004) found up-valley winds in their idealised simulation even for a valley with vertical slopes. In a valley with vertical slopes the taken cross section would be equal in the valley and above a plain. The subsidense warming in the valley core, caused by the slope wind circulation, modifies the vertical structure of CBL that forms an up-valley wind. Rampanelli et al. (2004) proposed this subsidence warming of the valley air to be the main driver of the valley winds, instead of the air volume difference introduced earlier.

2.2.3 Cross-valley winds and vertically stacked circulation

The cross-valley and vertically stacked circulation processes go beyond the standard textbook mechanisms, but are important to understand when monitoring the local mountain winds.

Cross-valley winds blow perpendicular to valley-axis from slope-to-slope and are moderately weak in magnitude (Whiteman, 2000). Uneven heating between the slopes cause cross-valley winds and thus they happen during daytime, since the longwave radiative cooling is equal between the slopes in spite of the valley orientation. The most typical characteristics of cross-valley winds is a surface wind flowing towards the warmer slope and opposite direction higher within the valley atmosphere. Strongest cross-valley circulations are most likely to occur in east-west orientated valleys, since the heating difference between the slopes are then the highest (Rotach et al., 2015). In north-south orientated valleys the cross-valley circulations occur in early morning and late evening when the differential heating of the slopes is at the strongest (Weigel and Rotach, 2004).

Wagner et al. (2014) found in their idealised valley simulations that during the coupled period deep and narrow valleys favor to form multiple circulation cells separated by inversion layers within the valley (Figure 2.6b). Similar result is visible in idealised valley simulations by Schmidli (2013) and Serafin and Zardi (2010). The lower circulation cell acts within the CBL and is associated with the up-slope winds and corresponding subsidense flow above the valley center. The circulation in the upper cell is relatively weaker than in the lower one and it is caused by the thermally driven cross-valley winds at the crest height, having also a subsidence flow above the valley center. Wagner et al. (2015b) summarise that single cross-valley circulation form in valleys with crest height less than the ABL height over adjacent horizontally homogeneous land. For deeper valleys the valley inversion would separate the circulation cells into multiple layers. Although whether the stacked circulation occurs it is highly dependent in the background forcing and static stability of the ABL.

Weigel and Rotach (2004) studied local mountain winds in Riviera valley in Switzerland and identified two cross-valley circulations occuring in the particular valley. The valley bends just before the entrance into Riviera valley which creates curvature-induced secondary circulation in the valley entrance during afternoons, which is illustrated in Figure 2.8. When the strong up-valley wind flows through the bend, the potentially colder and thus heavier air is packed close to the outer slope, pushing the potentially warmer and thus lighter air towards the inner slope. The potentially warmer air rises and cold air sinks creating a cross-valley circulation from the outer slope to inner slope and corresponding reversed circulation higher in the valley atmosphere. Near the head of the valley the cross-valley circulation is thermally driven. In the afternoon the west facing slope (outer slope in the case of mouth of the valley) in sun lit and east facing slope shaded. Ascent in sun lit and descent in shaded slope creates a counter-clockwise circulation. This thermally
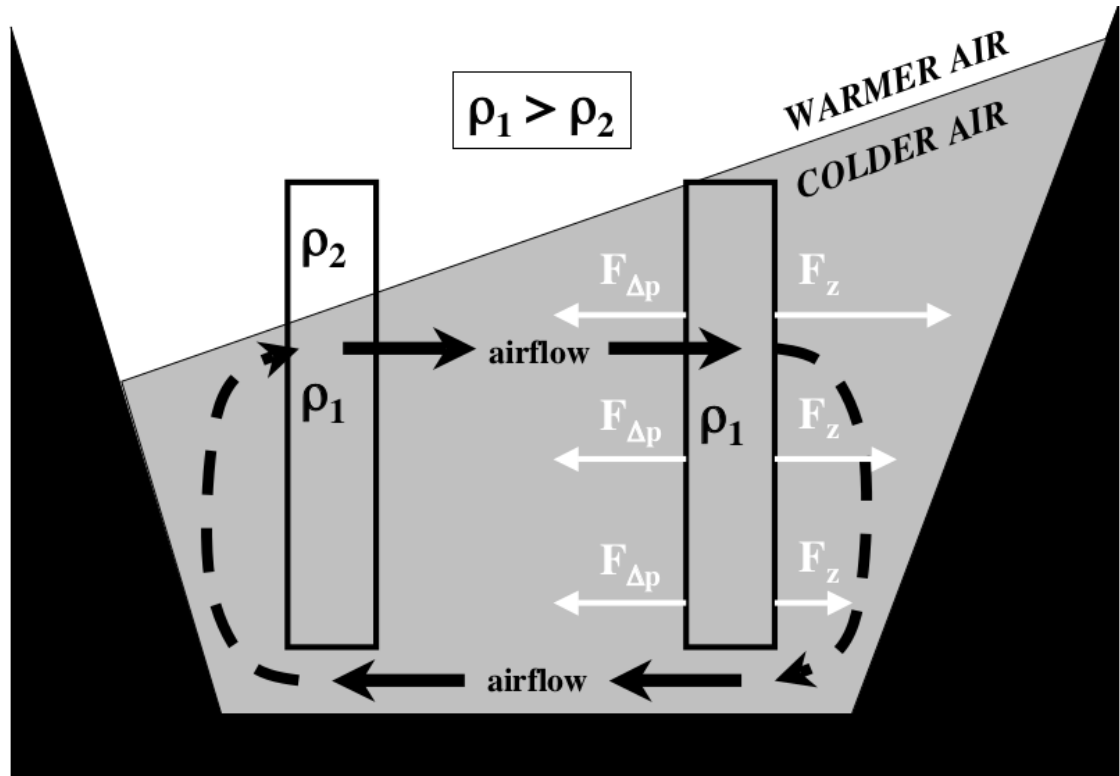
Figure 2.8: Daytime curvature-induced cross-valley circulation in the mouth of Riviera valley. Right-hand side is the outer slope and left-hand side is the inner slope. F_z and $F_{\Delta p}$ denote the centrifugal force and the hydrostatic pressure gradient force, respectively. Adapted from Weigel and Rotach (2004), Figure 11.

driven circulation is dominated by the curve-induced circulation in the mouth of the valley creating a clockwise circulation.

2.3   Terrain forced flow

When air flow confronts a barrier on its path, the air is forced to either flow around or over the obstacle. The resulting flow field depends on various factors and often the air flow split vertically in both going over and around layers (Whiteman, 2000). The most important factors are flow velocity, barrier height and width, static stability of atmosphere and the orientation and shape of the barrier with respect to the flow

direction. While the air is forced to ascend over the mountain, adiabatic cooling and condensation takes place on windward slope (Markowski and Richardson, 2010).

The more stable the air layer is, the more work is required for lifting it over the barrier. This required amount of work refers to the flow velocity and cross-barrier pressure gradient, meaning that even a stable layer can be brought over a barrier with great wind velocity or pressure difference. Isolated peaks and flow-parallel orientated barriers are more likely to separate the flow around them than wide mountain walls perpendicular to the flow. Also the shape of the barrier has an effect, concave barrier lifts the air more efficiently than a convex barrier.

Flows going around mountain barriers are associated with jet-like increased wind velocities (Whiteman, 2000). One type of these jets is barrier jet, that form when stable low-level flow confronts mountain massif perpendicular to it. In this case if there would be a thin gap through the mountain barrier, the flow velocities through the gap would be increased. The velocities increase due to Bernoulli effect: the same mass flows through a smaller cross section which forces the flow velocity to increase. Synoptic scale pressure gradients have also impact on the flows through gaps, driving the flow towards lower pressures which is called pressure-driven channeling. Cold pools are easily formed if a stable and cold air mass confronts a mountain barrier with relatively low velocity or below a strong flow (Whiteman, 2000).

Flow over a barrier may result in the lee side as a severe wind velocities, mountain waves and significant warming by Föhn effect. Mountain waves and downslope windstorms are introduced in the following Sections 2.3.1 and 2.3.2.

2.3.1   Mountain waves

Topography induced gravity waves form when stable air is brought over a mountain barrier (Whiteman, 2000). Air is forced to rise along the mountain wall resulting displaced vertically from its equilibrium level in a stable atmosphere. Due to grav-

a)   b)
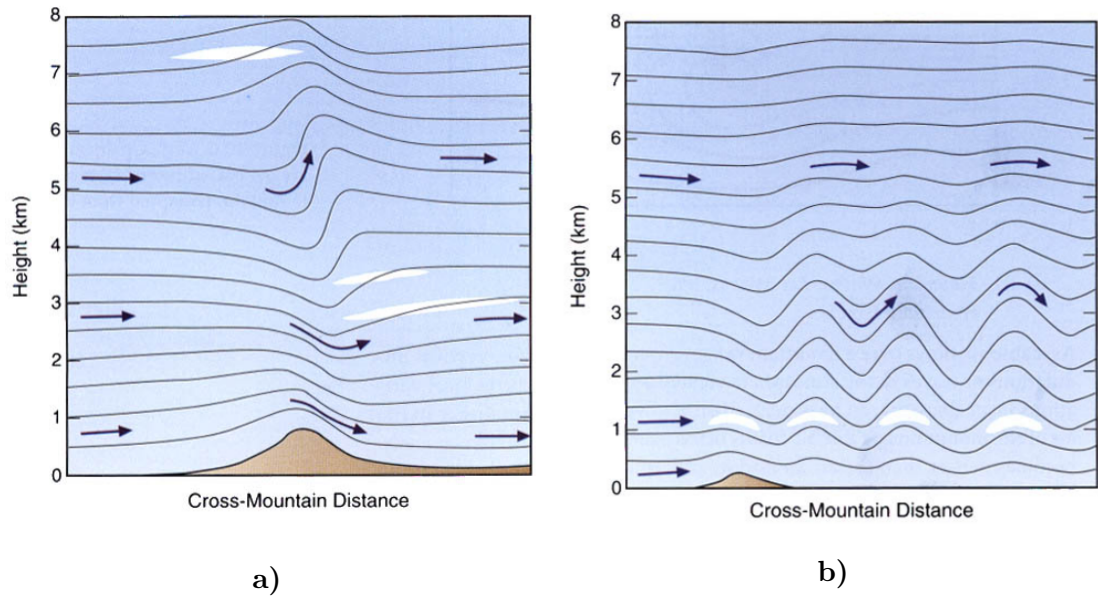
Figure 2.9: a) Vertically propagating wave. b) Trapped lee wave. Arrows refer to the flow direction and solid lines to the streamlines. White shading denote the probable clouds if the air is sufficient moist. Adapted from Whiteman (2000), Figures 10.8 and 10.9.

ity acting on the air, caused by vertical density anomaly, it is forced to descend. Reaching its equilibrium level the air has still momentum downwards causing it to overshoot and then be forced to rise again. This vertical oscillation around the equilibrium level is transported by the horizontal flow. Gravity waves formed by mountains are called mountain waves, buoyancy waves, lee waves and orographic waves (Holton and Hakim (2013), Markowski and Richardson (2010), Whiteman (2000)). The wave forms over the mountain, lee side or both (Whiteman, 2000). Depending on the atmospheric stability profile and wind shear the waves can either be trapped or verticaly propagate.

Trapped lee waves propagate downwind with a decreasing amplitude and range from low altitudes to mid-troposphere (Figure 2.9b). These waves require strong vertical wind shear and increasing stability to trap the gravity wave below the strong flowing stable layer (Holton and Hakim, 2013). The wavelength and amplitude of

trapped lee waves increase with a increasing horizontal flow velocity (Whiteman, 2000).

Vertically propagating mountain waves form with increasing stability without significant wind shear (Holton and Hakim, 2013). These waves can reach up to upper troposphere or even in stratosphere (Figure 2.9a). The highest amplitudes are found in middle troposphere and the highest surface wind velocities in the downslope flows in the lee side. The wider the mountain is, the more likely the wave is to propagate vertically (Markowski and Richardson, 2010).

If the mountain wave faces another barrier it may be either amplified or cancelled, depending on the relation between the wavelength and the distance between the mountains (Whiteman, 2000). Generally the mountain waves are most prominent with steep, high and wide barriers perpendicular to the flow direction.

With sufficient moisture clouds would form in the wave crests, both downwind and upwind (Whiteman, 2000). Laminar lenticularis clouds are a clear sign that gravity waves are present. Mountain waves with longer wavelengths can be visible as a long, mountain parallel straight border in altostratus cloud, called chinook archs. Without these clouds present the gravity waves are not visible and therefore they can cause severe, unexpected turbulence for aircraft.

2.3.2   Downslope windstorms

Downslope windstorms blow in the lee side of the mountain and are associated with topography induced gravity waves (Whiteman, 2000). These windstorms may reach to severe wind velocities, up to 30 meters per second, causing damage to forests, buildings and aircraft. Wind maxima is often found in the base of the slope or slightly downwind.

Conditions for forming downslope windstorms are similar to gravity waves, and often the strongest downslope wind velocities are observed in a break of standing

cross-mountain wave (Markowski and Richardson, 2010). In addition gentle slope and absence of cold stable layer on the lee side and relatively low or even reverse wind shear favor increased downslope wind velocities (Markowski and Richardson, 2010). Strongly stable layer near a mountain top with a less stable air above are also favorable condition for a strong downslope windstorm. Downslope windstorms happen more likely in winter and in lee waves with large wavelenghts (Whiteman, 2000).
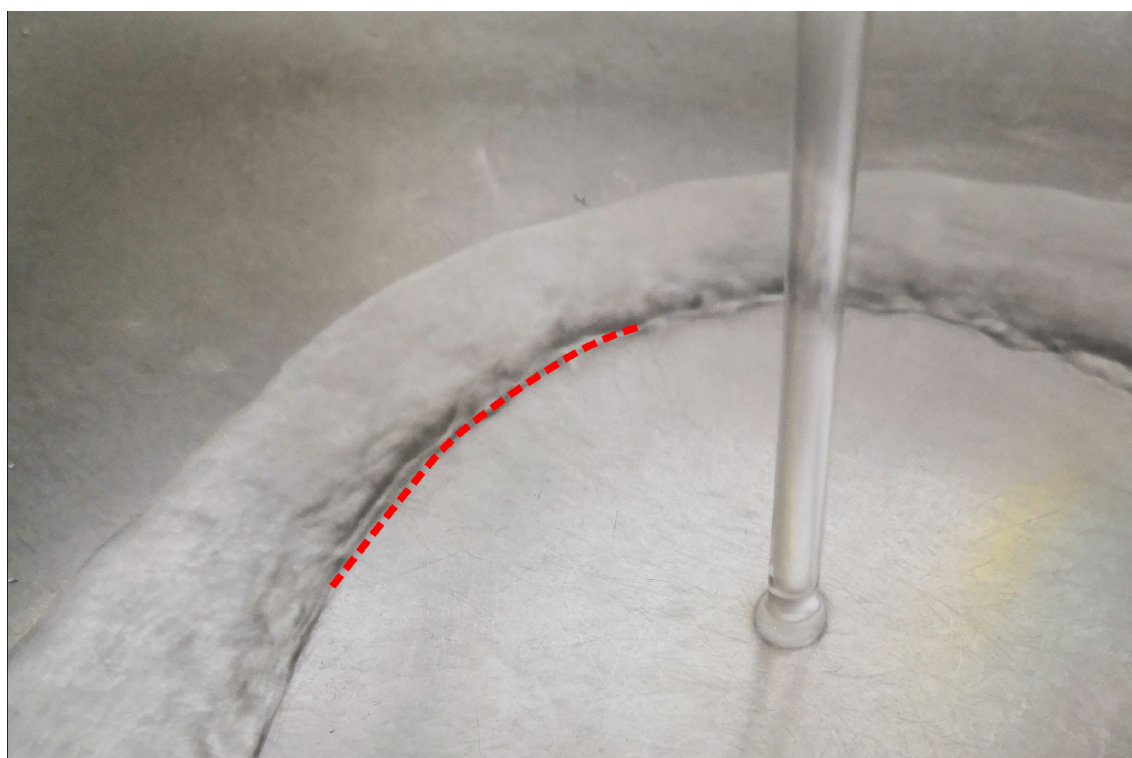
Figure 2.10: Hydraulic jump in water flow in a sink. Red dashed line denotes the boundary between laminar and turbulent flow, where the hydraulic jump takes place.

Often the strong gusty downslope winds have a structure of so called hydraulic jump (Markowski and Richardson, 2010). Hydraulic jump occurs downwind of an obstacle where is found an abrupt decrease in flow velocity and increase in fluid layer height. Same phenomenom occurs for water and can be illustrated with a water flow in a sink (Figure 2.10). Hydraulic jump takes place where the laminar flow becomes turbulent and the water height is increased. The mean velocity of the

fluid layer, towards the original direction, decreases but the turbulent motion cause increased wind velocity in gusts. These gusts cause severe wind speeds in downslope windstorms in case of hydraulic jump.

2.4 Khumbu valley

This thesis investigates the slope and valley winds in the Khumbu valley, that is located in Eastern Nepal, Central Himalayas. The Himalayas range all the way of 2500 kilometers from Pakistan in the west to Myanmar in east with a north-south width around 200 kilometers (Wester et al., 2019). The Khumbu valley is orientated in north-south direction, arising from less than 1000 meters above sea level towards the Nepal Climate Observatory-Pyramid station (NCO-P) marked with black star in Figures 2.12 and 3.2. NCO-P is in the base of Mount Everest at 5079 meters above sea level. Bollasina et al. (2002) describes the meteorological observations during 1994-1999 in NCO-P. Automatic weather station in NCO-P has measured air temperature, precipitation, wind speed and direction, atmospheric pressure and solar irradiance since December 1993.

Climate of the Khumbu valley is characterised by the annual cycle of summer monsoon, post-monsoon, dry season during winter and pre-monsoon (Bollasina et al., 2002). Bollasina et al. (2002) identified the onset and decay of summer monsoon to take place in mid-June and turn of October, respectively. Gautam and Regmi (2014) identified that the onset and withdraw of Indian monsoon are delayed after year 1997 and they are non-stationary year-to-year. Winter is defined to last from December to February, leaving the months of March to May and October to November for pre-monsoon and post-monsoon, respectively.

Due to the large range of elevations, the annual mean temperatures vary along Khumbu valley from more than 16°C to less than -4°C (Karki et al., 2016). Karki et al. (2016) classified the Nepal area using Köppen–Geiger climate classification.

Lower elevations of Khumbu valley are classified as Temperate climate with warm summer (Cwb[1]) and Cold climate with dry winter and warm summer (Dwb[2]). Higher elevations of Khumbu valley are classified as Polar Tundra (ET) or Polar Frost climate (EF), having warmest month temperature above and less than zero, respectively. In the Central-Eastern Himayalas over 80 percent of annual precipitation is brought by summer monsoon (Figure 2.11, Bookhagen and Burbank (2010)) and most of the winter precipitation are associated with synoptic scale weather disturbances (Wester et al., 2019). At elevations greater than 4800 meters above sea level the winter temperatures are below freezing and most of the precipitation is snow. During the summer monsoon the daily variation of temperature deacreases to 7 °C being rarely higher than 10 °C while during the winter the daily temperature varies 12 °C on average, some days even up to 20 °C (Bollasina et al., 2002). The decrease in daily temperature variations is caused by increased amount of clouds that decreases the daily heating and nocturnal cooling.

---

[1]**C** – Coldest month temperature above -3°C but less than +18 °, **w** – driest month precipitation in winter is less than wettest month precipitation in summer, **b** – at least four months temperature above 10 °C but less than 22 °C

[2]**D** – Coldest month temperature less than -3 °C)
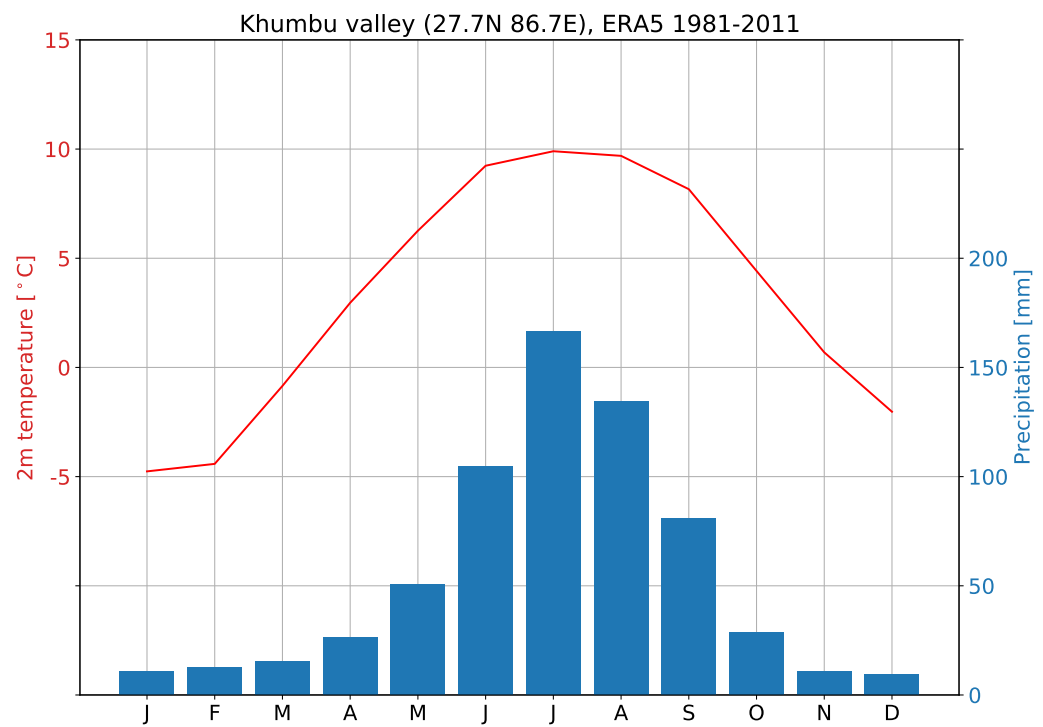
Figure 2.11: Climate diagram for Khumbu valley (27.7N 86.7E), period 1981-2011. 30 years monthly averages calculated using ERA5 reanalysis data (Muñoz Sabater, 2019).
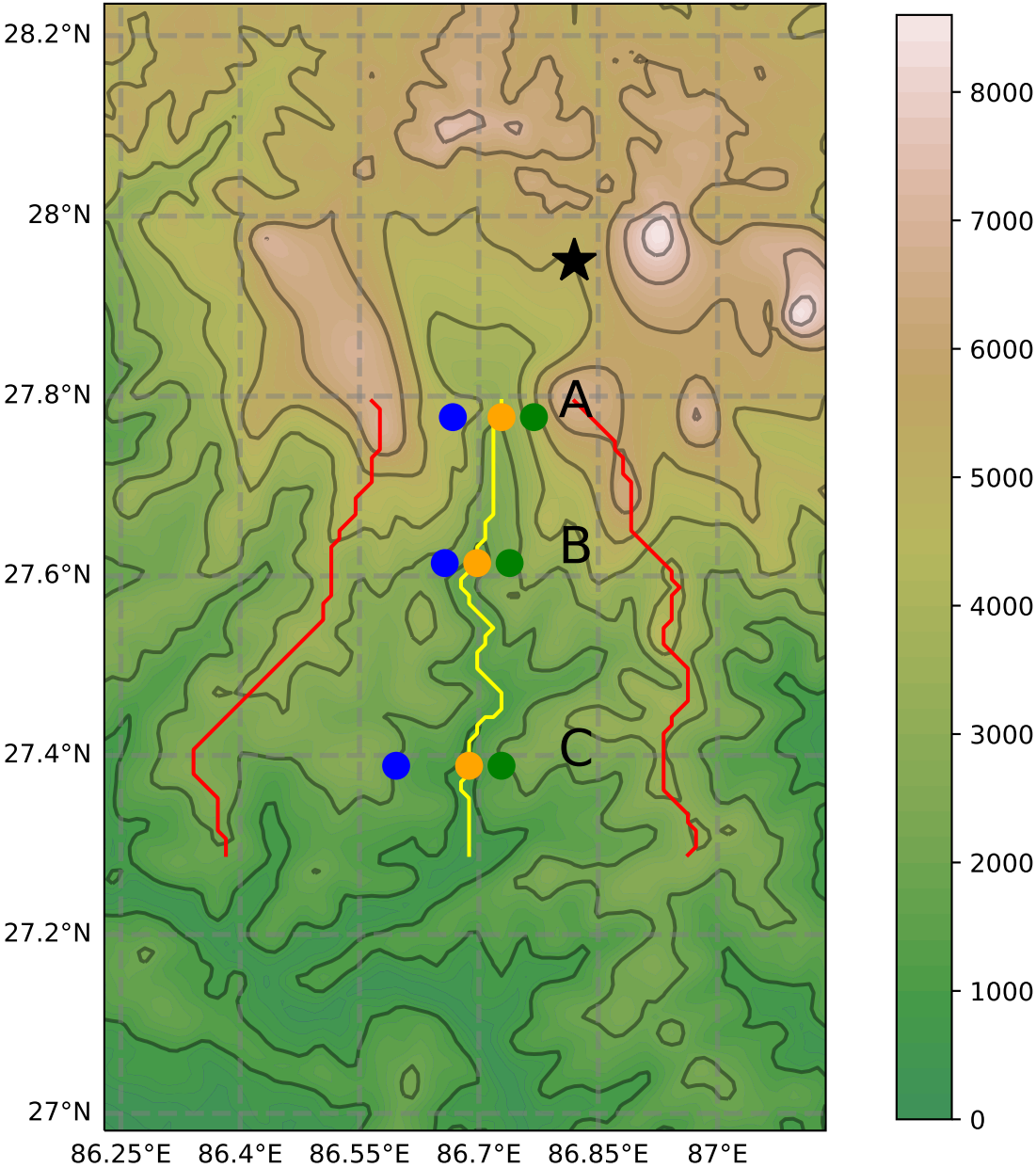
Figure 2.12: Khumbu valley as seen in WRF topography. Thick contours mark each 1000 meters above sea level. Valley center line and ridge lines marked with yellow and red, respectively. Nepal Climate Observatory-Pyramid station marked with star. Letters A-C mark different parts of the valley that will be examined in Chapters 4 and 5.

3. Methods

Slope and valley winds in the Himalayas were studied by using Weather Research and Forecasting model. First, the model will be introduced and later in Section 3.2 the particular run setup will be desrcibed.

3.1   Weather Research and Forecasting model

The Weather Research and Forecasting model (WRF) is a widely used numerical weather prediction model in research and operational meteorology (Powers et al., 2017). After it was first published in December 2000, registered users from over 160 countries had published up to 3000 WRF related articles by the end of 2015. The community of users have developed a wide range of parametrizations and applications, for example WRF-Chem (Wang et al., 2016) and HWRF (Bernardet et al., 2015), that could be used for air-quality and hurricane forecasting, respectively.

WRF is a fully compressible and nonhydrostatic model (Skamarock et al., 2008). The user can either choose the core with mass-based vertical coordinate that refers to ARW (Advanced Research WRF) or WRF-NMM (Nonhydrostatic Mesoscale Model) with hybrid-pressure coordinates (Powers et al., 2017). The height-based core was replaced with NCEP's (National Center for Environmental Prediction) Nonhydrostatic Mesoscale Model in the early stages of WRF. Janjic (2003) estimated a 20% increase in computational cost when nonhydrostatic verti-

cal motion were taken to account but beneficial accuracy between the cores were found even for a coarse resolution as 8 kilometers.

In addition to a wide range of spatial and temporal scales, WRF offers some great add-ons for research purposes (Powers et al., 2017). WRF has capability to run nested domains, where the inner domains could have higher resolution in the same simulation. WRF has good data assimilation options to initialize simulations with reanalysis data. In addition WRF has some idealised scenarios to simulate, such as flow over idealised topography or supercell convection.

Related to this study, WRF has been successfully used in studying thermally driven winds with idealised valley topographies (Leukauf et al. (2015), Leukauf et al. (2016), Wagner et al. (2015b), Catalano and Cenedese (2010), Giovannini et al. (2014b)). Giovannini et al. (2014b) concluded that according to their analyses, WRF is a reliable tool for simulating the local thermally driven winds in Alpine valleys. In their studies the WRF run at 500 meter resolution had errors comparable to Large-Eddy Simulation (LES) on 150 meter resolution. WRF simulations using resolutions 2 and 1.2 kilometers in Giovannini et al. (2014a) also managed to produce the diurnal valley winds well, the finer resolution ending up in some over estimation of valley wind magnitudes during evenings.

3.2   Model setup

The simulation used in this study is equal to one used in Bianchi et al. (2020). The simulation was done using WRF version 3.6.1.

The simulation was run with four nested domains that are presented in Figure 3.1. Domain d01 refers to the parent domain and d02, d03 and d04 to the inner domains. The parent domain covers area of 3618 kilometers by 2997 kilometers and the inner most d04 covers area of 300 kilometers by 288 kilometers. The nested domains have horizontal grid spacing of 27, 9, 3 and 1 kilometers and each domain
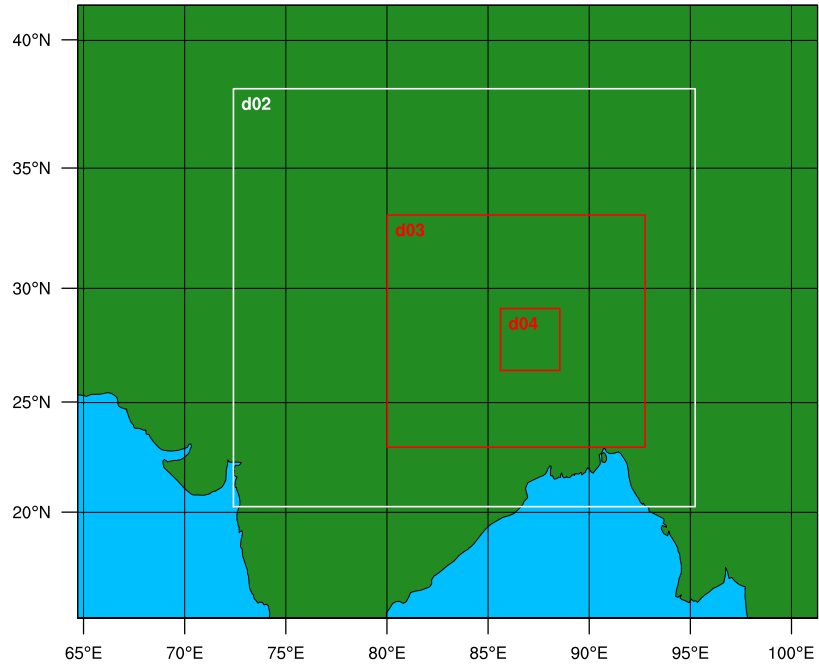
Figure 3.1: d01, d02, d03 and d04 domains in WRF simulation.

has 61 vertical levels. The simulation covers a five day period from 17th Dec 2014 to 21st Dec 2014 and the model output is given every half an hour in the inner-most domain d04. As described in Section 2.4, during December the dry winter season prevails in Khumbu valley which is favorable for studying the thermally driven winds. The summer monsoon reduces the daily temperature variations in Khumbu valley (Bollasina et al., 2002) which also is seen in the thermally driven winds by reduced surface wind magnitudes (Ohata et al., 1981)

The simulation was initialized with Climate Forecast System Reanalysis (Saha et al., 2010) that has a horizontal resolution of 0.5 degrees. To keep the simulation on track, it was nudged towards the reanalysis, which is available from each 6 hours. Nudging was performed for atmosphere above ABL. The surface topography data
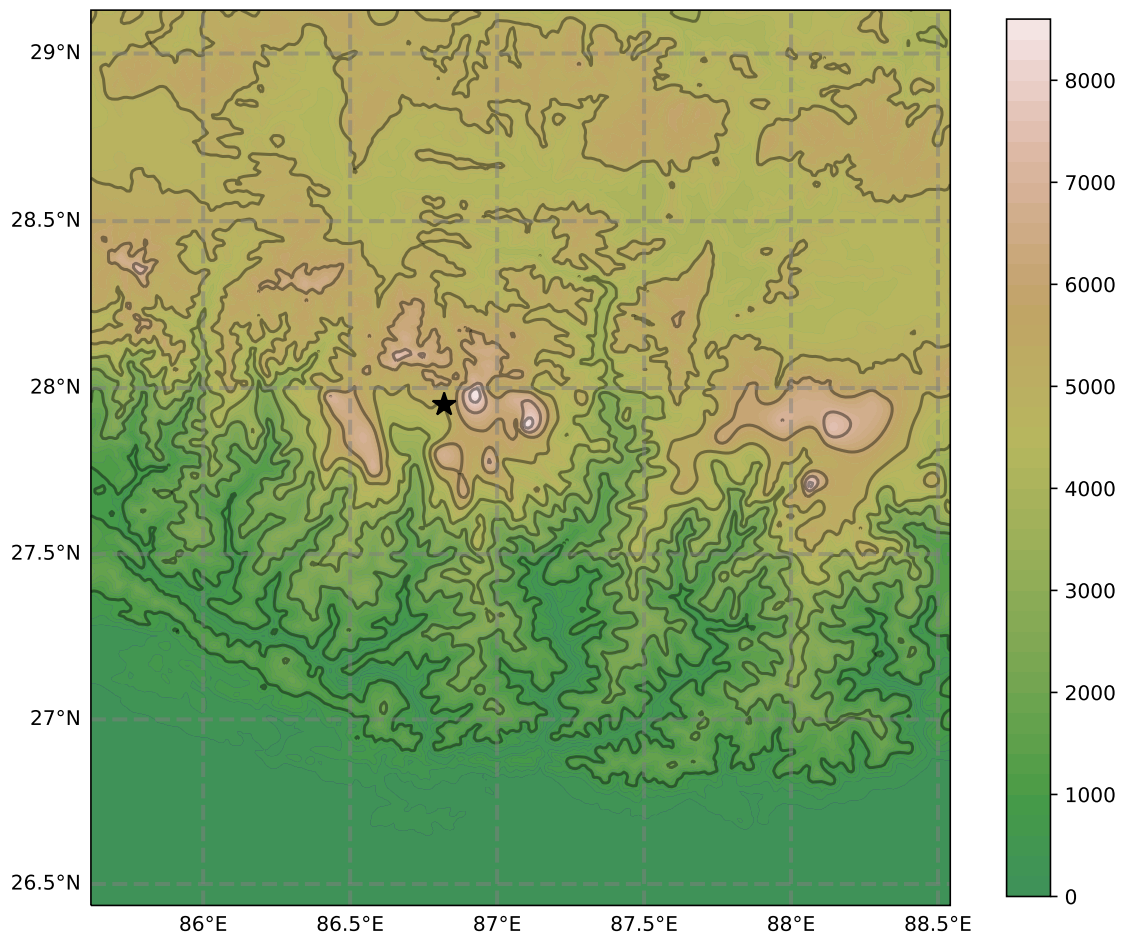
Figure 3.2: WRF simulation inner domain topography. Thick contours mark each 1000 meters above sea level. Nepal Climate Observatory-Pyramid station marked with star. NCO-P is located in 27.95°N, 86.82°E at 5079 meters above sea level near Mount Everest base camp.

is from United States Geological Survey (USGS) that has a horizontal resolution of 30 arc seconds, which means approximately one kilometer.

To keep the high resolution simulation numerically stable, adaptive timestep was calculated using a Courant-Friedrichs-Lewy (CFL) criteria of 0.8. CFL criteria limits the timestep to be small enough, so the fastest moving actions won't travel further than one grid spacing in a time step (Laney, 1998). For inner most domain d04 this means typically timestep of one second. To prevent refraction of waves there was used 6th order numerical diffusion and w-Rayleigh damping for the upper-most 5 kilometers. Microphysical phenomenas that happen on sub-grid length scales

are parametrized with Thompson scheme. Longwave and shortwave radiation are parametrized with RRTMG scheme on each 5 timesteps to save on computational costs. Turbulence in boundary layer is parametrized with Mellor-Yamada-Jenjic (Eta) TKE (turbulent kinetic energy) scheme and surface layer physics with Monin-Obukhov scheme.

According to recent studies, WRF is capable model to simulate the thermally driven mountain winds using 1 kilometer horizontal resolution (Giovannini et al. (2014b), Giovannini et al. (2014a), Potter et al. (2018), Collier and Immerzeel (2015), Karki et al. (2017)). Two studies using similar model setup than this thesis (WRF, 1 km horizontal resolution, USGS topography data) covering Khumbu valley showed that WRF simulates the local circulations well in this area (Potter et al. (2018), Karki et al. (2017)). Collier and Immerzeel (2015) stated that WRF using 1 kilometer resolution is not accurate enough to resolve the thermally driven winds in the narrowest parts of valleys (< 2 km) in Langtang Catchment, 150 kilometers west from Khumbu valley. This limit will reduce the reliability of the model setup in the narrowest valleys that branch east from the main Khumbu valley, thats shown by the yellow line in Figure 2.12. According to the comparison of high resolution WRF and observations on studies in the Alps (Giovannini et al. (2014b), Giovannini et al. (2014a)) and in the Himalayas (Potter et al. (2018), Collier and Immerzeel (2015), Karki et al. (2017)) this model setup is suitable for studying the slope and along-valley winds in Khumbu valley, that has ridge-to-ridge distance from 25 to 50 kilometers (ridge lines shown by red lines in Figure 2.12).
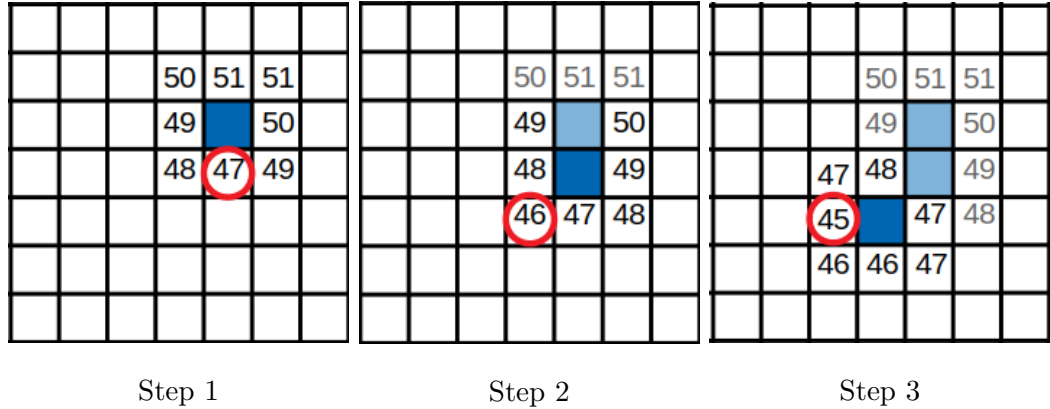
Figure 3.3: Valley center line identification algorithm. Numbers refer to surface height in the grid points. Dark blue squares refer to the grid point at the valley center line where the algorithm is at each step. Red circle points the grid point which is selected by the algorithm on each step. Light blue squares refer to the grid points already saved in the valley center line.

3.3 Data analysis

Slope and along-valley winds in this simulation were examined by timeseries and cross section plots. For studying the slope and along-valley wind components, the wind vector was separated into two components. Although the Khumbu valley is north-south oriented (Figure 2.12), the meridional and zonal components did not describe the along-valley and slope wind in each point so those components were calculated for each plot. The methodology to do this is described in following sections 3.3.1 and 3.3.2.

3.3.1 Valley center line identification

To identify the along-valley wind component, one must know the valley orientation in the model grid. The valley center line, that is shown by yellow line in Figure 2.12, was identified from the WRF topography field with the script in Appendix A. Figure 3.3 describes how the algorithm works step by step. The algorithm starts from a given grid point at the head of the valley (dark blue square in Step 1 in

Figure 3.3), searching and saving the route to the mouth of the valley. In each step the code picks the lowest height in the surrounding grid points and continues the procedure from that grid point (red circle in Figure 3.3). In case the valley center line has local minima, the code checks if the lowest point is already saved in the valley center line. This prevents the algorithm getting stuck looping in the same local minima. With a little modification, the same code was used for identifying the ridge lines, that are shown in Figure 2.12 by the red lines.

3.3.2 Valley and slope wind components

Wind vector $\vec{V}$ is expressed by using zonal and meridional wind components, u and v in cartesian coordinates:

$$\vec{V} = u\hat{x} + v\hat{y} \tag{3.1}$$

Along-valley wind component, V_a, is a component of wind vector pointing towards the local tangent of valley center line. Vector $\vec{A}$ marks the vector from grid point $(n-2)$ to $(n+2)$ at the nth grid point on the valley center line.

$$\vec{A} = \hat{x}(x_{n+2} - x_{n-2}) + \hat{y}(y_{n+2} - y_{n-2}), \tag{3.2}$$

where (x, y) marks the grid points of valley center line. With this notation, vector $\vec{A}$ points upvalley so V_a being positive marks upvalley wind. V_a in grid point n is now calculated by taking dot product of wind vector and unit vector of $\vec{A}$.

$$
\begin{aligned}
V_a &= \hat{A} \cdot \vec{V} \\
V_a &= \frac{\vec{A} \cdot \vec{V}}{|\vec{A}|} \\
V_a &= \frac{u(x_{n+2} - x_{n-2}) + v(y_{n+2} - y_{n-2})}{\sqrt{(x_{n+2} - x_{n-2})^2 + (y_{n+2} - y_{n-2})^2}}
\end{aligned}
\tag{3.3}
$$

Slope wind component, V_s, is the perpendicular component to along-valley wind. The wind direction will be also compared to the actual height gradient of the slope

in Chapter 4. With this notation and in the case of Khumbu valley, up-slope wind on the east slope is positive and down-slope wind negative, and vice versa for the west slope. Slope wind component can be calculated by using the valley vector $\vec{A}$:

$$
\begin{aligned}
V_s &= \left(\hat{k} \times \hat{A} \right) \cdot \vec{V} \\
V_s &= \left(\hat{k} \times \frac{\vec{A}}{|\vec{A}|} \right) \cdot \vec{V} \\
V_s &= \frac{u(y_{n+2} - y_{n-2}) - v(x_{n+2} - x_{n-2})}{\sqrt{(x_{n+2} - x_{n-2})^2 + (y_{n+2} - y_{n-2})^2}}
\end{aligned}
\tag{3.4}
$$

Slope and along-valley wind timeseries are presented in a way that positive (negative) values refer to up-slope (down-slope) and up-valley (down-valley) winds. In cross section plots perpendicular to the valley axis the slope winds follow the aforementioned notation, that at the east (west) slope the up-slope wind is positive (negative) and down-slope wind is negative (positive).

4. Results

This chapter answers to the research question: Are the slope and valley winds driven by the textbook mechanisms in Khumbu valley? Slope wind mechanisms is caused by horizontal temperature differences in the vicinity of the surface and valley wind mechanism by the air volume difference along the valley. These theories were described in details in Sections 2.2.1 and 2.2.2. The results will be discussed in Chapter 5.

In Figures 4.1–4.7 the panels A, B and C refer to different parts of the valley that are shown in Figure 2.12. The locations A, B and C refer to the head, middle part and the mouth of the Khumbu valley, respectively. Blue, orange and green timeseries refer to west slope, valley center and east slope, respectively. The grid points shown in orange are picked from the valley center line (Section 3.3.1) and the grid points on the slopes are picked from same latitude with approximately same surface height. The variables in timeseries are plotted every half an hour, which is the model output timestep of the simulation. The timeseries are plotted on local time, which is in Nepal +5:45UTC. The shaded grey areas denotes the hours between sunset and sunrise.
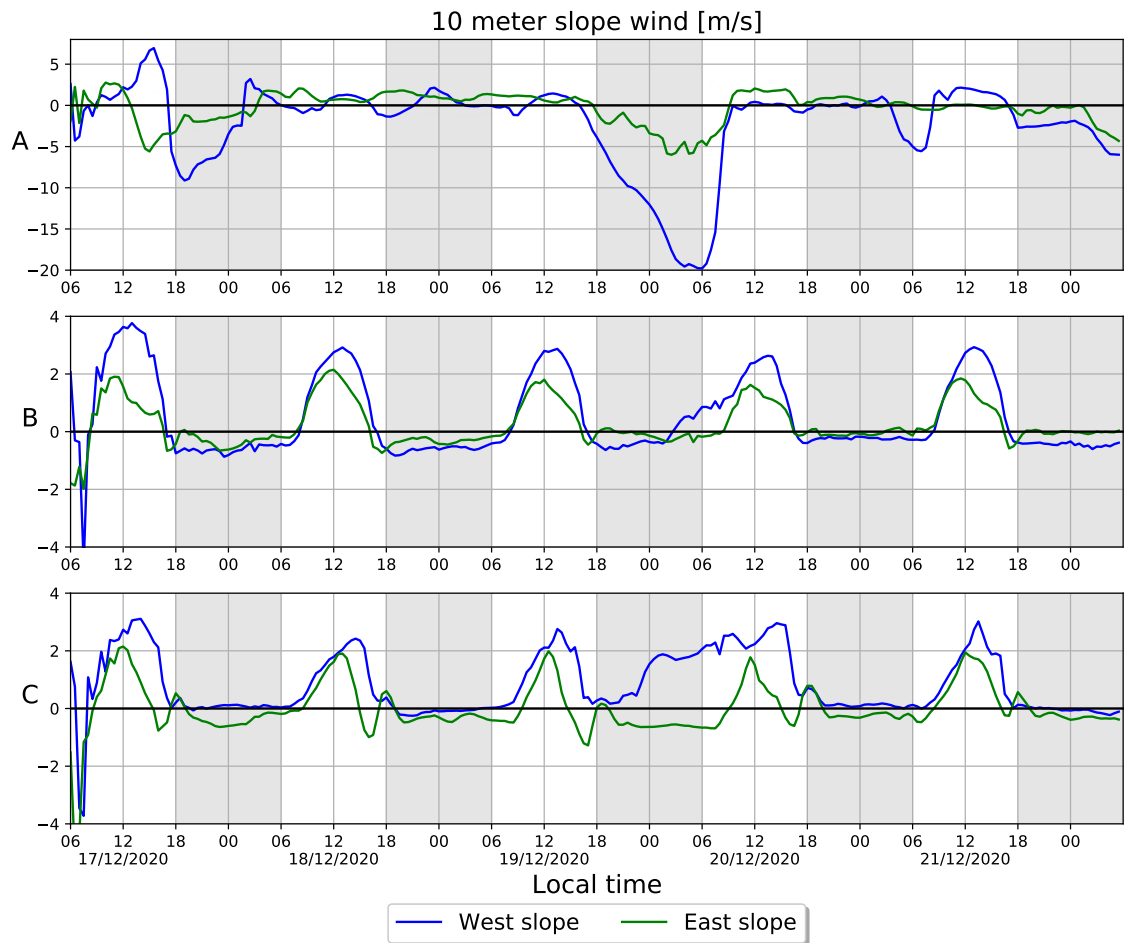
Figure 4.1: Timeseries of 10 meter slope wind in Khumbu valley. Positive values mark upslope wind and negative values downslope wind. Time between sunset and sunrise shaded on gray. Panels A-C refer to different parts of Khumbu valley shown in figure 2.12. Note that the scale of vertical axis in panel A differs from B-C.

4.1   Slope winds in Khumbu valley

In lower and middle parts of the Khumbu valley the 10 meter slope winds have a textbook daily cycle with daytime up-slope winds and nighttime down-slope winds (Figure 4.1B–C). The up-slope winds peak their maxima in the afternoon and have a maximum magnitude of 2–3 meters per second. The up-slope winds are mainly stronger at the west slope compared to the east slope having peak magnitudes 0.5 to 1 meters per second greater. Nocturnal downslope winds are weaker, having a

average magnitude less than 1 meter per second. In the upper part of the Khumbu valley (Figure 4.1A) the 10 meter slope wind does not have that clear daily cycle. The west slope shows some signs of thermally driven up-slope winds during the second, third and last day of the simulation but otherwise the slope winds do not have the similar patterns than in the lower and middle parts of Khumbu valley. The slope winds in the upper part of the valley are dominated by synoptic scale wind channelling and by a mountain wave developing into the valley.
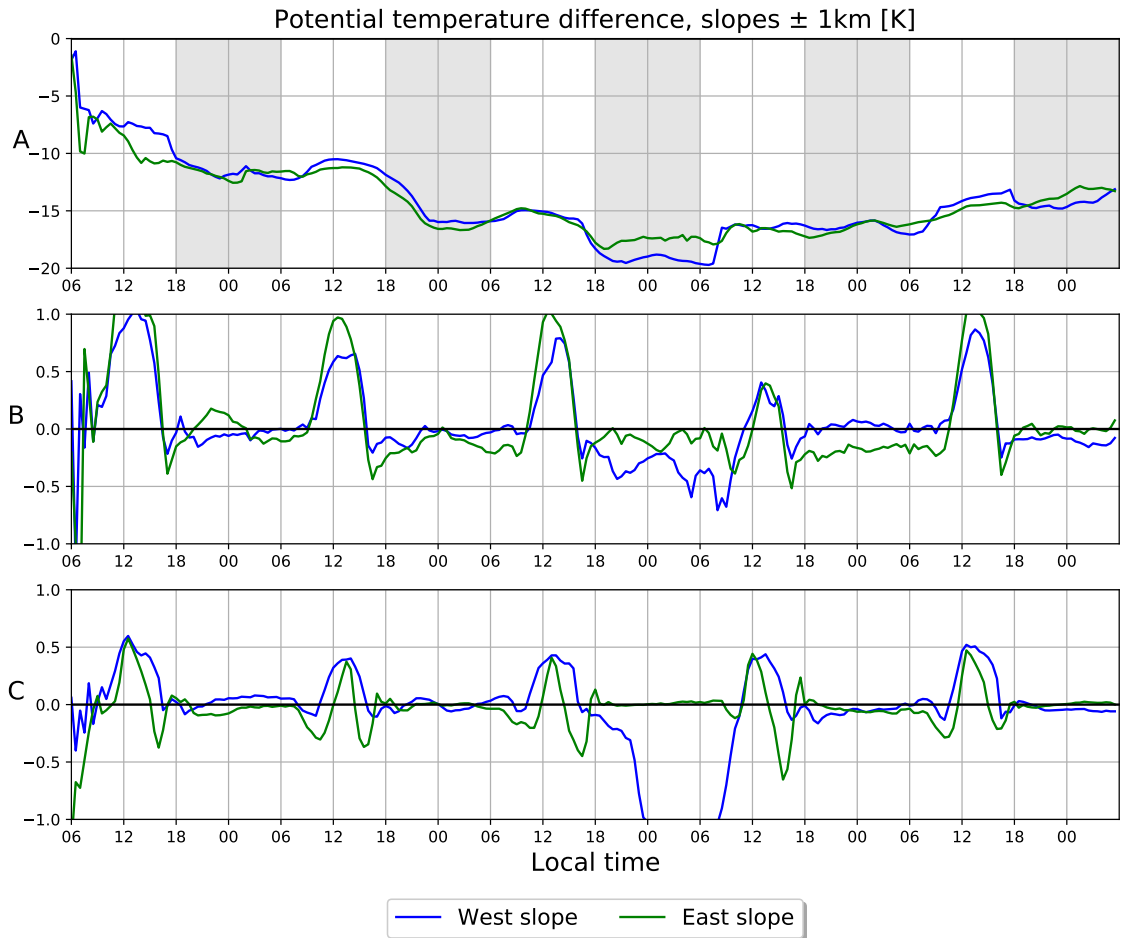
Figure 4.2: Timeseries of potential temperature difference between the slope surface and next grid point towards valley center at the same height. Panels A-C refer to different parts of Khumbu valley shown in Figure 2.12

According to the textbook slope wind mechanism, the slope winds are driven by the horizontal temperature differences at the vicinity of the slope surface (Whiteman (2000), Markowski and Richardson (2010)). In Figure 4.2 is shown the horizontal potential temperature differences at the Khumbu valley slopes. The difference is calculated using the lowest vertical level at the slope grid points (shown in Figure 2.12) and the next grid point towards the valley center interpolated at the same height. Positive values mean that the air closer to the slope is warmer. The lowest vertical level is on average 25 meters above the slope surface, but this method was the most accurate for avoiding the use of extrapolation in the potential temperature profiles. As told in Section 2.2.1 the 25 meters is more likely to be within the well developed up-slope wind layer that has a depth of 50 to 150 meters but it does not show the strongest horizontal temperature differences found just at the surface, especially during the morning and evening transition periods.

Comparing the timeseries of 10 meter slope wind magnitude (Figure 4.1) and the horizontal potential temperature difference at the slope surface (Figure 4.2) one can say there is a relation with the daytime cycles. The temperature difference peak at the same time with peaking up-slope wind. So can be stated that the up-slope winds are driven by textbook mechanism in the lower and middle parts of the Khumbu valley. The nocturnal temperature differences are small, caused by their examination at the 25 meter height, and can not be said if the down-slope winds are driven by the slope wind mechanism. Figure 4.3 shows the 10 meter wind direction timeseries at the slopes. The solid lines present the direction of height gradient in the grid points denoting the direction of pure slope wind mechamism driven slope wind. In the middle and lower parts of the valley at the west slope the 10 meter wind actually flow towards the height gradient referring to thermally driven slope winds. At the east slope the wind direction is towards the height gradient only at the noon, when the slope wind mechanism is at its strongest.
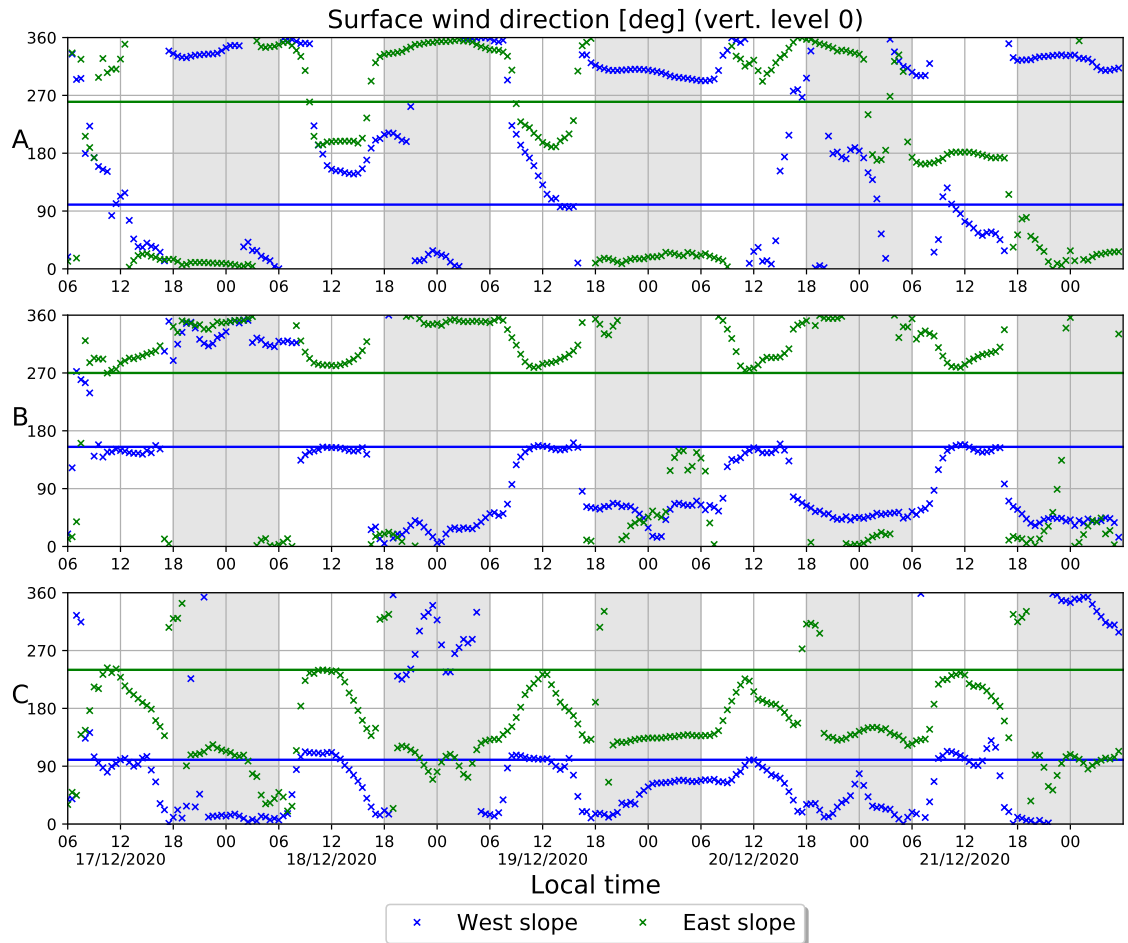
Figure 4.3: Timeseries of wind direction on slope surfaces. Solid lines denote the direction of surface height gradient. Panels A-C refer to different parts of Khumbu valley shown in Figure 2.12

The difference in slope wind magnitudes between the west and east slopes could be explained with the location of selected grid points. In the mouth of the valley (Figure 4.1C) the grid point at the west slope is further away from the valley axis. Slope wind magnitude increases with distance which would explain the 1 meter per second difference between the peaking up-slope wind magnitudes. In the middle part of the valley (Figure 4.1B) some portion of the up-slope wind might be advected by up-valley winds before the valley axis turns east.

Third night of the simulation is exceptional as there is up-slope winds at the west slope. Compared to other nights in the lower parts of the valley there is a
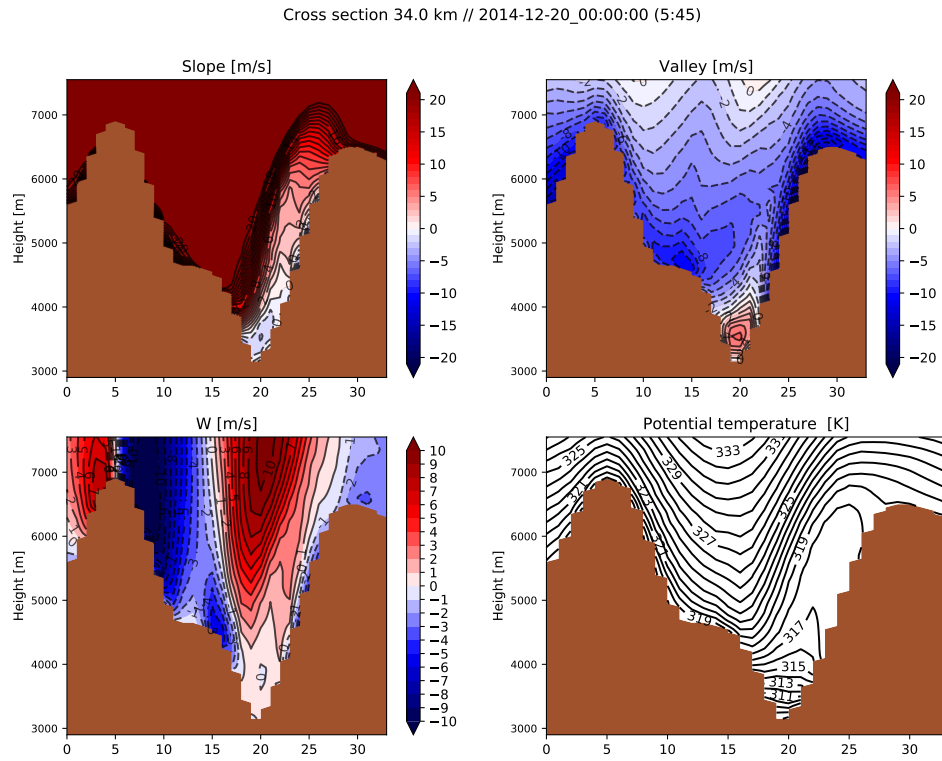
Figure 4.4: Ridge-to-ridge cross section of the head of Khumbu valley (A in Figure 2.12) on 20th Dec 2014 5:45 local time. Upper left, upper right, lower left and lower right panels show the slope wind, along-valley wind, vertical wind and potential temperature profiles, respectively. Slope wind is shown in the notation described in Section 3.3.2, positive (negative) slope wind referring to wind component towards right (left) and positive (negative) along-valley wind referring to up-valley (down-valley) wind. Horizontal axis is in kilometers meaning the shown ridge-to-ridge topography profile is shown steeper as it is in reality.

stronger inversion layer developing at the crest height below the strong western winds and there is a stronger up-valley wind blowing in the residual layer above the valley floor (not shown). Also there is down-valley wind flowing at the west slope (Figure 4.5C) which could indicate for cold air advection from the higher altitudes resulting in the drop in surface temperature (Figure 4.2C).

The ridge-to-ridge cross section of the gravity wave developing, around the part of A in Figure 2.12, is shown in Figure 4.4 (more timesteps shown in Figures 1–3 in

Appendix B). The development of the gravity wave started when synoptic scale wind direction turns to west. Then the wind flows more perpendicular to the northwest-southeast orientated cliff on the west side of the head of the valley. Large scale wind flowing perpendicular to a high and wide barrier is likely condition for forming a gravity wave, which is seen just in the case of the head of the Khumbu valley in this simulation. The gravity wave structure is seen in the potential temperature profile having a wave-like structure and also in the vertical wind component. Flow pattern in this gravity wave has also characteristics of hydraulic jump, which would explain the strong surface winds in the west slope.
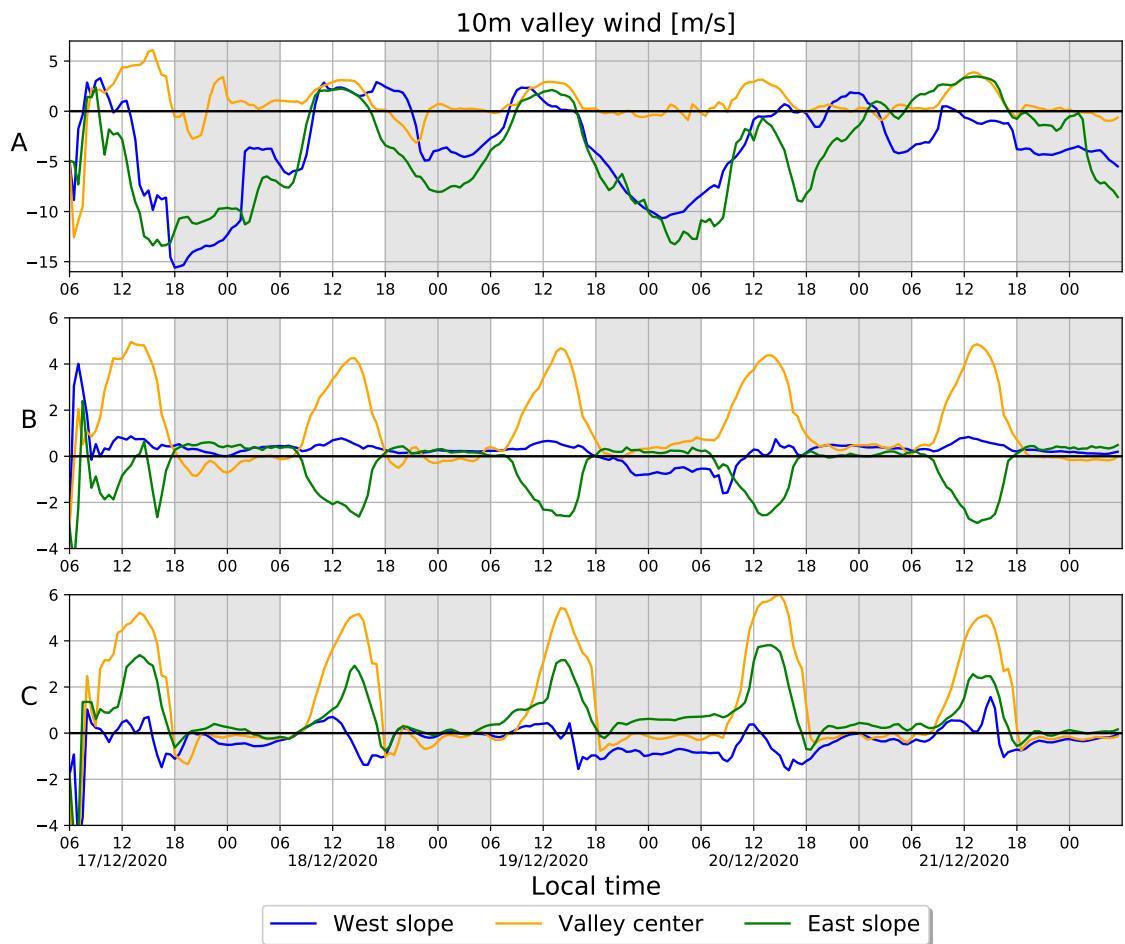
Figure 4.5: 10 meter along-valley wind in Khumbu valley. Positive values mark upvalley wind and negative values downvalley wind. Panels A-C refer to different parts of Khumbu valley shown in Figure 2.12. Note that the scale of vertical axis in panel A differs from B-C.

4.2 Along-valley winds in Khumbu valley

Along the center line of the Khumbu valley (yellow line in Figure 2.12) there is a textbook cycle of daytime up-valley winds, as seen in 10 meter along-valley wind timeseries in Figure 4.5. The up-valley winds develop after the sunrise and peak in the afternoon around 15 local time and is ceased at the time of sunset around 18 local time. Nocturnal along-valley winds are relatively weak, around less than 0.5 meters per second flowing up or down-valley.

In the lower part of the valley the daytime up-valley winds are stronger on the eastern slope than on the western slope (Figure 4.5C). This could be caused by both the selection of grid points and the valley geometry. The daily up-valley wind in the slopes depends on the distance from the valley center line, the closer to the valley center the stronger the along-valley wind component would be. The grid point on the eastern slope is closer to the valley center than the grid point on the western slope. The Khumbu valley also bends near the mouth of the valley (Figure 2.12). The curvature induced jet (described in Section 2.2.3) increases the up-valley winds in the outer slope, which is in this case the eastern slope. The structure of along-valley wind jet is seen in the cross section plot as the tilt in the isotaches (Figure 4 in Appendix B).

By textbook mechanisms, along-valley winds are driven by valley wind mechanism that is caused by the air volume difference between the valley atmosphere and the air above a adjacent plain, or the air volume changes along the valley (Whiteman (2000), Markowski and Richardson (2010)). In case the valley floor is elevated along the valley axis the slope wind mechanism drives also the winds along the valley.

The air volume effect can be estimated from the valley geometry. In Figure 2.12 is presented the valley ridge lines on red. The Khumbu valley narrowes towards the head of the valley, by looking at the distance of the ridge lines to each other. In addition to narrowing the Khumbu valley also steepens, which can be seen in ridge-

to-ridge height profiles (not shown), which affects the ABL height as described in Section 2.1.1. When estimating the air volume that is warmed by the solar radiation, there should be compared the ABL air volume along the valley, because the portion of atmosphere affected by Earth surface is defined as the ABL. In Figure 4.6 is calculated the ABL cross sectional area along the valley floor for each latitude around the valley center line separated for daytime and nighttime. Technically the ABL cross section area is an integrated area between the WRF model topography and model boundary layer height. To ensure the equal horizontal area for the comparison the ABL cross section is calculated 5 kilometers around the valley center line.
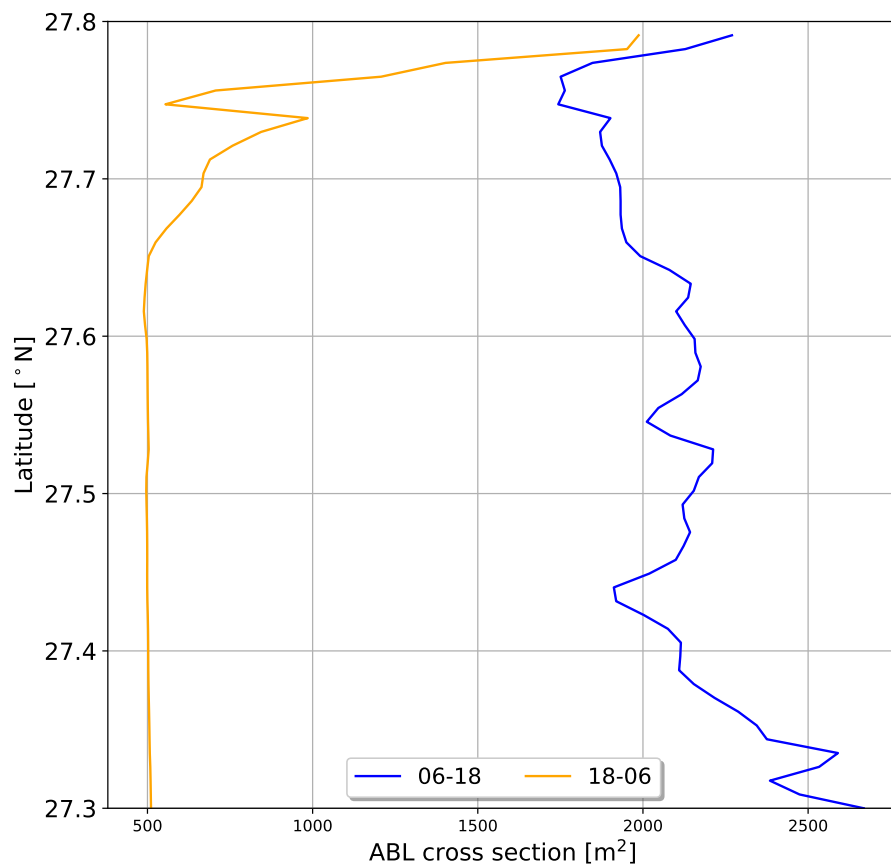
Figure 4.6: Area between the surface and ABL height along the Khumbu valley for the horizontal area 5 kilometers around the valley center line. Blue and orange line denotes the mean value for the daytime (06-18 local time) and nighttime (18-06 local time) during the five days simulation. ABL height is the boundary layer height from the model output.

During daytime the ABL volume decreases from the mouth of the valley towards the middle part of the valley. In the head of the valley the ABL air volume increases again caused by the valley opening and strong winds near the surface (Figures 4.1A and 4.5A). During nighttime there is no ABL air volume differences along the valley except the increase in the head of the valley compared to rest (Figure 4.7). Overall the nocturnal ABL height is very low. The decrease in the magnitude of along-valley wind maxima towards the head of the valley is probably caused by the decrease in the ABL air volume differences.
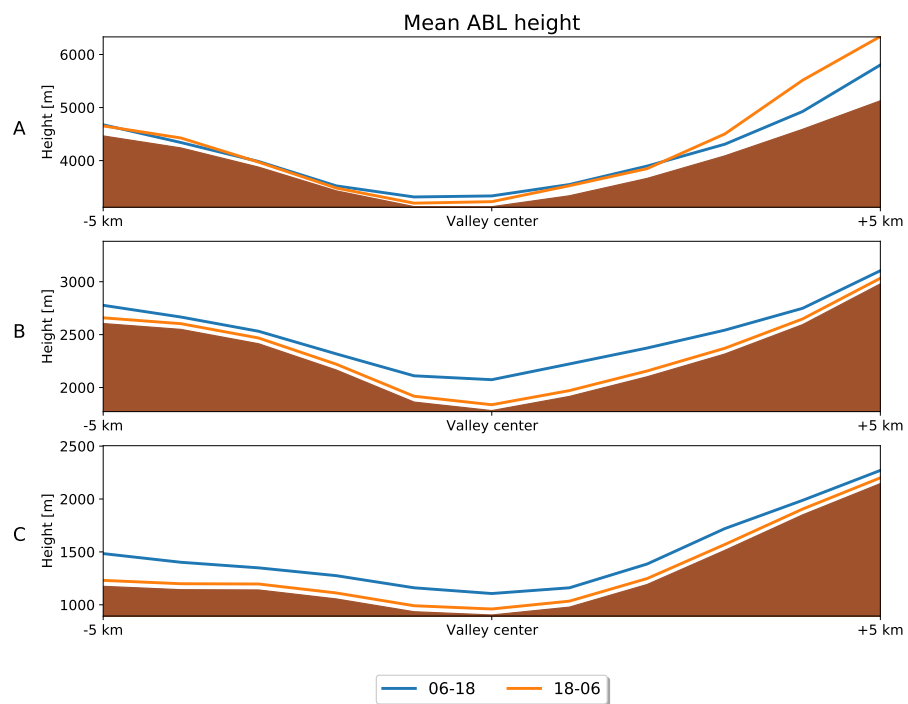
Figure 4.7: Mean height of the atmospheric boundary layer separated for daytime (06-18 local time) and nighttime (18-06 local time) shown on blue and orange, respectively. ABL height is the boundary layer height from the model output. Panels A-C refer to different parts of Khumbu valley shown in Figure 2.12. Note that the scale of vertical axis in panel A differs from B-C.

In Figure 4.8 is the potential temperature profile in along-valley cross section as a snapchot from the second noon of the simulation. Comparing this Figure 4.8 to the textbook sketch of the potential temperature profile for developing a up-slope wind in Figure 2.4a (Section 2.2.1) there is a clear similarity. Horizontal isentropes

turn downwards in the vicinity of the surface which causes the air at the surface to be accelerated up the valley. During nighttime the inclination of isentropes that would drive the down-slope winds are not found in the cross sections (not shown).
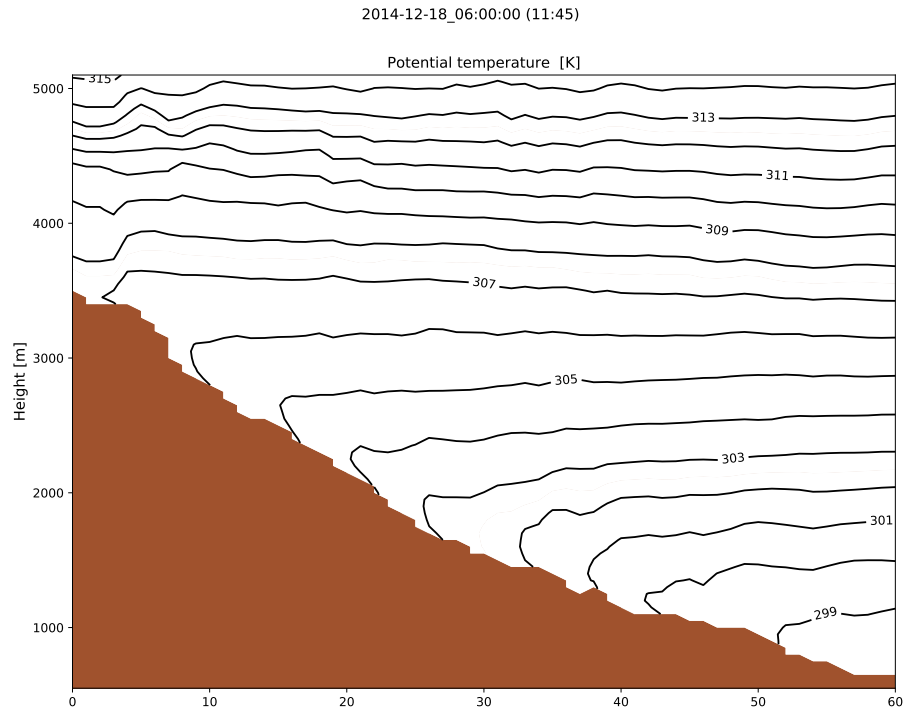
Figure 4.8: Potential temperature profile on a cross section along the Khumbu valley as a snapshot of the second day noon (local time 11:45) of the simulation. The horizontal axis is the valley center line shown with yellow line in Figure 2.12 and the numbers refer to horizontal distance in kilometers.

In Khumbu valley the daily up-valley winds are driven by the textbook mechanisms. Valley and slope wind mechanisms are caused by valley narrowing and inclination towards the head of the valley, respectively. The nocturnal down-valley winds are weak and the analysis does not advocate that the textbook mechanisms for down-valley winds are relevant.

5. Discussion

In this chapter the results and methods used in this study are compared to similar studies and literature on the topic. Few studies have investigated the local wind patterns in Khumbu valley using observations or simulations. The observation network in Khumbu valley is not comprehensive, having less than 10 automatic weather stations nowadays in the upper part of the valley. All the observation based studies in Khumbu valley are concentrated in the valley center line so there really is no in-situ observations to compare from the slopes, which is probably caused by the logistical issues in the mountainous area.

Both the studies using observations (Ohata et al. (1981), Shea et al. (2015), Ueno et al. (2008), Inoue (1976)) and simulations (Potter et al. (2018), Karki et al. (2017)) result in strong daytime up-valley winds and weak or absent nocturnal along-valley winds in Khumbu valley. Strong up-valley winds would be expected by the Khumbu valley geometry, as in Wagner et al. (2015b) was studied the enhancement of up-valley wind magnitudes by valley narrowing and floor inclination. Similar along-valley wind pattern is seen in the simulation of this study and also the presence of both slope and valley wind mechanisms in the daytime along-valley winds.

Potter et al. (2018) studied the dynamical drivers of the local winds in Khumbu valley, with similar WRF setup than in this study. Their simulation was done using same horizontal resolution and topography data but the microphysical parameterizations were partly different and there was 50 vertical levels in their simulation,

whereas in this study the simulation has 61 vertical levels. They found strong daytime along-valley winds that continued throughout the nighttime as weaker up-valley winds and textbook daily cycle for slope winds. The simulated slope and along-valley winds are similar than in this study. The lack of nocturnal down-valley winds in this analysis may be caused by the fact that the down-valley wind layer is typically shallow so it would not be seen in the 10 meter winds. Potter et al. (2018) found that pressure gradient force was the strongest driving force of the winds with some influence of advection. This seems also consistent with the role of textbook mechanisms in the simulations used in this study.

Potter et al. (2018) found also in their simulation characteristics of orographic waves in the head of the valley. The same was seen in the simulation used in this study on the third night and day that can be seen in increased 10 meter winds up to 20 meters per second. The simulation of this study is not valitated with comparison on observations which limits the reliability of the results. Especially in the extremely strong downslope wind speeds in the western slope in the head of the valley, where the gravity wave acts on. The mountain wave development can be seen in Figure 4.4 and in Figures 1–3 in Appendix B.

Shea et al. (2015) found in their observation based study that the daily wind maxima is typically found around 15 and 16 local time in Khumbu valley. Their find is consistent with this study as the along-valley wind maxima is found in the afternoon each day of the simulation. They also found that the wind speed magnitude is a function of the station location in relation to the main valley axis in this area (including two different valleys nearby). This can be seen in lower part of the valley in Figures 4.1C and 4.5C as the wind speeds at the east slope are greater than at the west slope, where the grid point examined is further away from the valley center.

The boundary layer height used for estimating the ABL air volume, in the case of valley wind mechanisms, was WRF output ABL height. Banks et al. (2015) found in their study that WRF systematically underestimates the ABL height. Herrera-Mejía and Hoyos (2019) evaluated the ABL height estimation of WRF in a narrow and complex valley. Their result was that WRF has a high skill in ABL height estimation with better results over the valley floor than over the slopes. This combined with the unclear definition of ABL height over complex terrain (de Wekker and Kossmann, 2015) might cause an error in the analysis of Figure 4.6. Although the along-valley wind magnitudes decrease with decreasing difference in ABL air volume, the error might only be seen in the absolute values calculated for the ABL cross section areas.

6. Conclusions

Slope and valley winds in the Himalayan valley were studied using a high resolution weather simulation. The model used in this study is Weather Research and Forecasting model (WRF) which were run for 5 days period in December 2014 at 1 kilometer horizontal grid spacing and 61 vertical levels in the area of Mount Everest in the Nepal Himalayas. This thesis concentrates in the Khumbu valley which is a approximately 120 kilometers long valley leading to the west base of Mount Everest from the south. The aim of this thesis is to determine if the slope and valley winds are driven by textbook mechanisms in the Khumbu valley.

The daily cycle of local mountain winds in Khumbu valley were similar to what the earlier studies done in this valley stated. The 10 meter slope winds have a textbook diurnal cycle in the lower and middle parts of this valley. The up-slope winds reach their maxima at noon with magnitudes of 2 to 3 meters per second and turn down-slope around sun set with weaker magnitudes less than 1 meter per second. In the head of the valley the 10 meter slope winds are dominated by synoptic scale wind channelling and gravity wave developing into the valley. Slope wind mechanism was studied by comparing horizontal potential temperature differences at the vicinity of the slope surface with the slope wind component. The daily cycles were similar and therefore can be said that the slope wind mechanism is present in the form of the daily up-slope winds.

The daily up-valley wind in the center line of the Khumbu valley has a textbook cycle of developing after sun rise, peaking at afternoon and ceasing around sun set. During nighttime the along-valley winds are weak, mostly less than 0.5 meters per second. The role of valley wind mechanism was studied from the valley geometry of Khumbu valley but also by estimating the air volume within atmospheric boundary layer along the valley. The air volume of atmospheric boundary layer decreased from the mouth of the valley towards the middle parts of the valley, especially in the lower parts of the valley, where the up-valley winds are the strongest. Slope wind mechanism is also acting along the valley axis because the Khumbu valley is elavated steeply towards the head of the valley. Both valley and slope wind mechanisms were stated to be driving the daytime up-valley winds due to valley narrowing and elavation towards the head of the valley, respectively.

The simple textbook mechanisms for thermally driven slope and valley winds were found to work partly in the simulation using high resolution in grid spacing and topography data. The relatively recent, more complex and detailed additions in these theories were found to work in the valley geometry and curvature induced flow patterns. The future work will include extension of the analysis in the other major valleys of the Nepal Himalayas and combination of aerosol physics and chemistry with the high resolution meteorological modelling.

Acknowledgements

First I want to thank my supervisor Victoria Sinclair for all the advice and expertise during this thesis work. Thank you for being such supportive supervisor during the years I have worked in your guidance! Second, I want to thank my supervisor Federico Bianchi for being able to work in his project. I am looking forward to continue the work with both of you!

Many thanks to the Dynamic meteorology group in the Insititute for Atmospheric and Earth system Research. Thank you for all the feedback in my thesis presentations and for the warm atmosphere in the research group. Special thanks for all the fellow students in the meteorology courses and in the meteorology student organisation Synop ry. Thank you for all the joy and challenges we have went through these years.

Last, I want to thank Tiia for all the love and support at home and our four-legged friend, Vilho, for the company during the remote work days.

Appendix A. Valley center line identification code

The code is written in `Python 3`.

```python
#x,y is the given grid point on top of the valley
#hgt is the topography field in (x,y) coordinates
#resulting valley center line is valley_x,valley_y
#from head of the valley towards the mouth of the valley
x, y = x_start, y_start
for n in range(0,20):
    hgt_tmp = []
    for i in [-1,0,1]:
        for j in [-1,0,1]:
            if i==0 and j==0:
                continue
            if n > 4:
                if valley_x[-3] == x+i or valley_x[-2] == x+i:
                    if valley_y[-3] == y+j or valley_y[-2] == y+j:
                        continue
                else:
                    hgt_tmp.append(hgt[x+i,y+j])
                    if min(hgt_tmp) == hgt_tmp[-1]:
                        x_tmp, y_tmp = x+i, y+j
            else:
                hgt_tmp.append(hgt[x+i,y+j])
                if min(hgt_tmp) == hgt_tmp[-1]:
                    x_tmp, y_tmp = x+i, y+j

    valley_x.append(x_tmp)
    valley_y.append(y_tmp)
    x, y = x_tmp, y_tmp
```
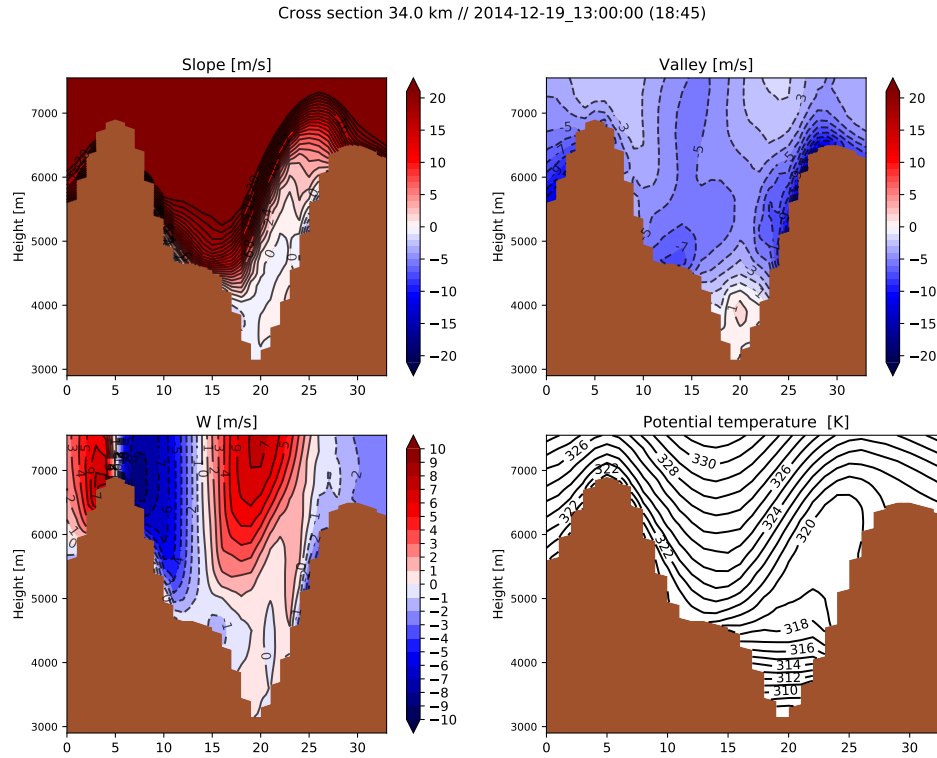
Appendix B. Valley cross section plots
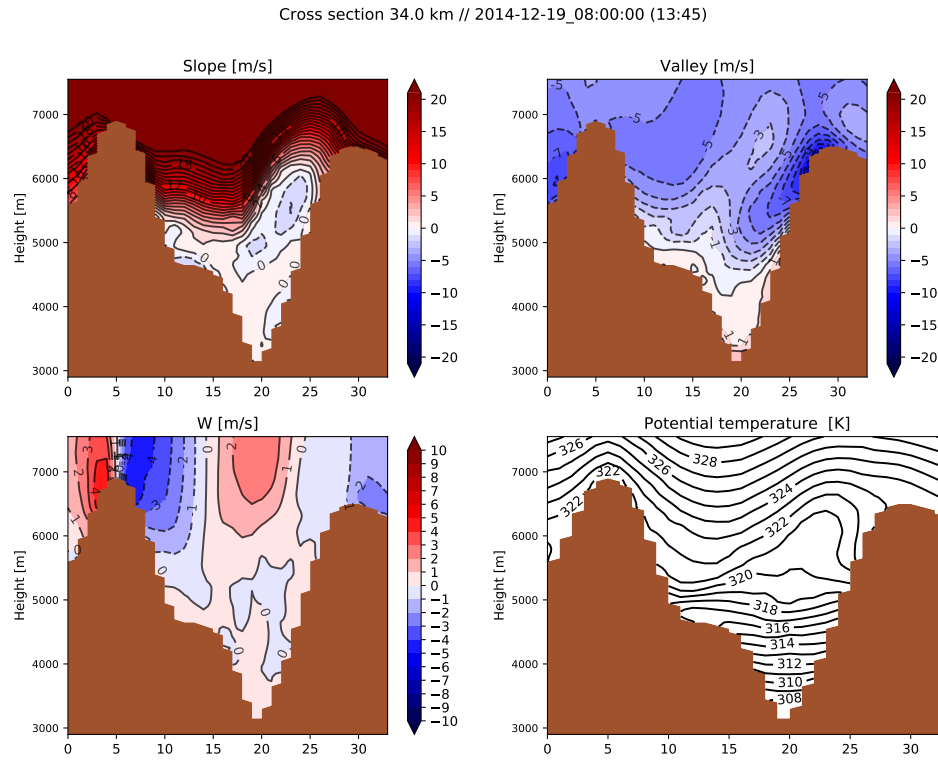
Figure 1: Ridge-to-ridge cross section from the head of Khumbu valley (A in Figure 2.12) on 19th Dec 2014 13:45 local time. Upper left, upper right, lower left and lower right panels show the slope wind, along-valley wind, vertical wind and potential temperature profiles, respectively. Slope wind is shown in the notation described in Section 3.3.2, positive (negative) slope wind referring to wind component towards right (left) and positive (negative) along-valley wind referring to up-valley (down-valley) wind. Horizontal axis is in kilometers meaning the shown ridge-to-ridge topography profile is not on scale.

Cross section 34.0 km // 2014-12-19_13:00:00 (18:45)
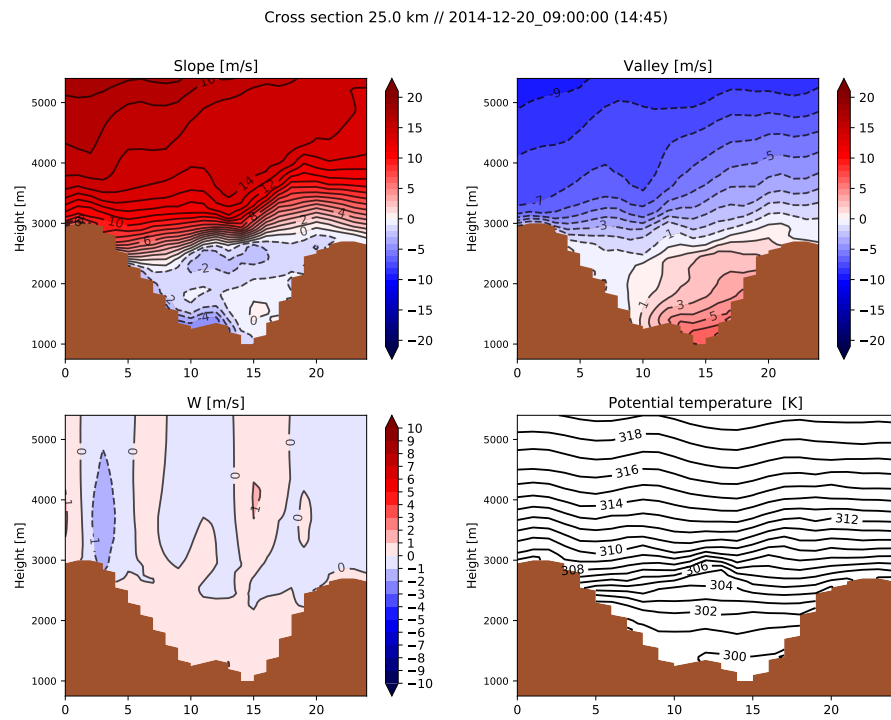
Figure 2: Ridge-to-ridge cross section from the head of Khumbu valley (A in Figure 2.12) on 19th Dec 2014 18:45 local time. Upper left, upper right, lower left and lower right panels show the slope wind, along-valley wind, vertical wind and potential temperature profiles, respectively. Slope wind is shown in the notation described in Section 3.3.2, positive (negative) slope wind referring to wind component towards right (left) and positive (negative) along-valley wind referring to up-valley (down-valley) wind. Horizontal axis is in kilometers meaning the shown ridge-to-ridge topography profile is not on scale.

Cross section 34.0 km // 2014-12-19_18:00:00 (23:45)
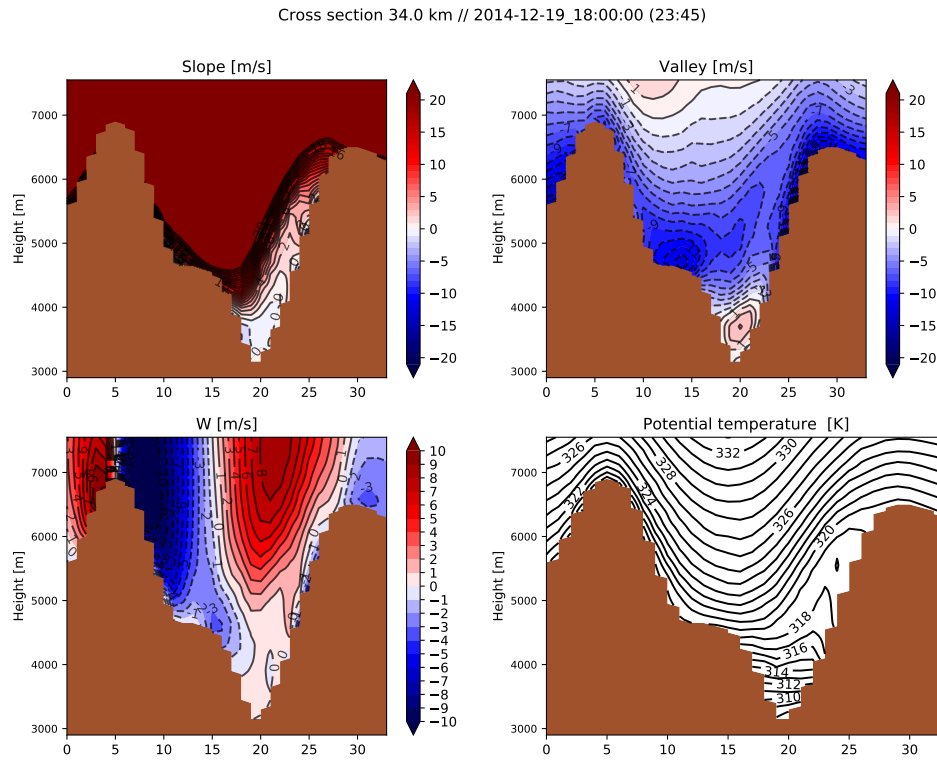
Figure 3: Ridge-to-ridge cross section from the head of Khumbu valley (A in Figure 2.12) on 19th Dec 2014 23:45 local time. Upper left, upper right, lower left and lower right panels show the slope wind, along-valley wind, vertical wind and potential temperature profiles, respectively. Slope wind is shown in the notation described in Section 3.3.2, positive (negative) slope wind referring to wind component towards right (left) and positive (negative) along-valley wind referring to up-valley (down-valley) wind. Horizontal axis is in kilometers meaning the shown ridge-to-ridge topography profile is not on scale.

Cross section 25.0 km // 2014-12-20_09:00:00 (14:45)

Figure 4: Slope-to-slope cross section from the mouth of Khumbu valley (C in Figure 2.12) on 20th Dec 2014 14:45 local time. Upper left, upper right, lower left and lower right panels show the slope wind, along-valley wind, vertical wind and potential temperature profiles, respectively. Slope wind is shown in the notation described in Section 3.3.2, positive (negative) slope wind referring to wind component towards right (left) and positive (negative) along-valley wind referring to up-valley (down-valley) wind. Horizontal axis is in kilometers meaning the shown ridge-to-ridge topography profile is not on scale.

Bibliography

Banks, R., Tiana-Alsina, J., Rocadenbosch, F., and Baldasano, J. (2015). Performance evaluation of boundary layer heights from lidar and the Weather Research and Forecasting model at an urban coastal site in the northeast Iberian Peninsula. *Bound.-Lay. Meteorol.*, 15:1–28.

Barry, R. G. (2008). *Mountain Weather and Climate.*, volume 3rd ed of *Routledge Physical Environment Series.* Cambridge University Press.

Bernardet, L., Tallapragada, V., Bao, S., Trahan, S., Kwon, Y., Liu, Q., Tong, M., Biswas, M., Brown, T., Stark, D., Carson, L., Yablonsky, R., Uhlhorn, E., Gopalakrishnan, S., Zhang, X., Marchok, T., Kuo, B., and Gall, R. (2015). Community Support and Transition of Research to Operations for the Hurricane Weather Research and Forecasting Model. *Bulletin of the American Meteorological Society*, 96(6):953–960. 10.1175/BAMS-D-13-00093.1.

Bianchi, F., Junninen, H., Bigi, A., Sinclair, V. A., Dada, L., Hoyle, C. R., Zha, Q., Yao, L., Ahonen, L. R., Bonasoni, P., Mazon, S. B., Hutterli, M., Laj, P., Lehtipalo, K., Kangasluoma, J., Kerminen, V.-M., Kontkanen, J., Marinoni, A., Mirme, S., Molteni, U., Petäjä, T., Riva, M., Rose, C., Sellegri, K., Yan, C., Worsnop, D. R., Kulmala, M., Baltensperger, U., and Dommen, J. (2020). Biogenic particles formed in the Himalaya as an important source of free tropospheric aerosols. *Accepted in Nature Geosciences.*

Bollasina, M., Bertolani, L., and Tartari, G. (2002). Meteorological observations at high altitude in the Khumbu Valley, Nepal Himalayas, 1994-1999. *Bull. Glaciol. Res.*, 19:1–11.

Bookhagen, B. and Burbank, D. W. (2010). Toward a complete Himalayan hydrological budget: Spatiotemporal distribution of snowmelt and rainfall and their impact on river discharge. *Journal of Geophysical Research: Earth Surface*, 115(F3). 10.1029/2009JF001426.

Catalano, F. and Cenedese, A. (2010). High-Resolution Numerical Modeling of Thermally Driven Slope Winds in a Valley with Strong Capping. *Journal of Applied Meteorology and Climatology*, 49(9):1859–1880. 10.1175/2010JAMC2385.1.

Collier, E. and Immerzeel, W. W. (2015). High-resolution modeling of atmospheric dynamics in the Nepalese Himalaya. *Journal of Geophysical Research: Atmospheres*, 120(19):9882–9896. 10.1002/2015JD023266.

De Wekker, SFJ. Steyn, D. and Fast, J. (2005). The performance of RAMS in representing the convective boundary layer structure in a very steep valley. *Environ Fluid Mech*, 5. https://doi.org/10.1007/s10652-005-8396-y.

de Wekker, S. and Kossmann, M. (2015). Convective Boundary Layer Heights Over Mountainous Terrain—A Review of Concepts. *Frontiers in Earth Science*, 3.

Diémoz, H., Barnaba, F., Magri, T., Pession, G., Dionisi, D., Pittavino, S., Tombolato, I. K. F., Campanelli, M., Della Ceca, L. S., Hervo, M., Di Liberto, L., Ferrero, L., and Gobbi, G. P. (2019). Transport of Po Valley aerosol pollution to the northwestern Alps – Part 1: Phenomenology. *Atmospheric Chemistry and Physics*, 19(5):3065–3095. 10.5194/acp-19-3065-2019.

Ekhart, E. (1948). De la structure thermique de l'atmosphere dans la montagne [On the thermal structure of the mountain atmosphere, English translation: White-

man, C.D., and Dreiseitl, E. (1984). Alpine Meteorology: Translations of Classic Contributions by A.Wagner, E. Ekhart and F. Defant.]. 10.2172/6665518.

Foken, T. (2008). *Micrometeorology.* Springer-Verlag Berling Heidelberg.

Gautam, D. and Regmi, S. (2014). Recent Trends in the Onset and Withdrawal of Summer Monsoon over Nepal. *ECOPERSIA*, 1:353–367.

Giovannini, L., Antonacci, G., Zardi, D., Laiti, L., and Panziera, L. (2014a). Sensitivity of Simulated Wind Speed to Spatial Resolution over Complex Terrain. *Energy Procedia*, 59:323–329. 10.1016/j.egypro.2014.10.384.

Giovannini, L., Laiti, L., Serafin, S., and Zardi, D. (2017). The thermally driven diurnal wind system of the Adige Valley in the Italian Alps. *Quarterly Journal of the Royal Meteorological Society*, 143(707):2389–2402. 10.1002/qj.3092.

Giovannini, L., Zardi, D., de Franceschi, M., and Chen, F. (2014b). Numerical simulations of boundary-layer processes and urban-induced alterations in an Alpine valley. *International Journal of Climatology*, 34(4):1111–1131. 10.1002/joc.3750.

Gohm, A., Harnisch, F., Vergeiner, J., Obleitner, F., Schnitzhofer, R., Hansel, A., Fix, A., Neininger, B., Emeis, S., and Schaefer, K. (2009). Air pollution transport in an alpine valley: Results from airborne and ground-based observations. *Boundary-Layer Meteorology*, 131. 10.1007/s10546-009-9371-9.

Herrera-Mejía, L. and Hoyos, C. D. (2019). Characterization of the atmospheric boundary layer in a narrow tropical valley using remote-sensing and radiosonde observations and the WRF model: the Aburrá Valley case-study. *Quarterly Journal of the Royal Meteorological Society*, 145(723):2641–2665. https://doi.org/10.1002/qj.3583.

Holton, J. R. and Hakim, G. J. (2013). *An Introduction to Dynamic Meteorology (Fifth Edition).* Academic Press, Boston, fifth edition.

Inoue, J. (1976). Climate of Khumbu Himal. 10.5331/seppyo.38.Special_66.

Janjic, Z. (2003). A nonhydrostatic model based on a new approach. *Meteorology and Atmospheric Physics*, 82:271–285. 10.1007/s00703-001-0587-6.

Karki, R., Talchabhadel, R., Aalto, J., and Baidya, S. (2016). New climatic classification of Nepal. *Theor Appl Climatol 125*.

Karki, R., ul Hasson, S., Gerlitz, L., Schickhoff, U., Scholten, T., and Böhner, J. (2017). Quantifying the added value of convection-permitting climate simulations in complex terrain: a systematic evaluation of WRF over the Himalayas. *Earth System Dynamics*, 8(3):507–528. 10.5194/esd-8-507-2017.

Laney, C. B. (1998). *Computational Gasdynamics*. Cambridge University Press. 10.1017/CBO9780511605604.

Leukauf, D., Gohm, A., and Rotach, M. W. (2016). Quantifying horizontal and vertical tracer mass fluxes in an idealized valley during daytime. *Atmospheric Chemistry and Physics*, 16(20):13049–13066. 10.5194/acp-16-13049-2016.

Leukauf, D., Gohm, A., Rotach, M. W., and Wagner, J. S. (2015). The Impact of the Temperature Inversion Breakup on the Exchange of Heat and Mass in an Idealized Valley: Sensitivity to the Radiative Forcing. *Journal of Applied Meteorology and Climatology*, 54(11):2199–2216. 10.1175/JAMC-D-15-0091.1.

Markowski, P. and Richardson, Y. (2010). *Mesoscale Meteorology in Midlatitudes*. 10.1002/9780470682104.

Muñoz Sabater, J. (2019). ERA5-Land monthly averaged data from 1981 to present. Copernicus Climate Change Service (C3S) Climate Data Store (CDS). (Accessed 19 Oct 2020).

Ohata, T., Higuchi, K., and Ikegami, K. (1981). Mountain-Valley Wind System in the Khumbu Himal, East Nepal. *Journal of the Meteorological Society of Japan. Ser. II*, 59(5):753–762. 10.2151/jmsj1965.59.5_753.

Orville, H. D. (1964). On Mountain Upslope Winds. *Journal of the Atmospheric Sciences.*

Potter, E. R., Orr, A., Willis, I. C., Bannister, D., and Salerno, F. (2018). Dynamical Drivers of the Local Wind Regime in a Himalayan Valley. *Journal of Geophysical Research: Atmospheres*, 123(23):13,186–13,202. 10.1029/2018JD029427.

Powers, J. G., Klemp, J. B., Skamarock, W. C., Davis, C. A., Dudhia, J., Gill, D. O., Coen, J. L., Gochis, D. J., Ahmadov, R., Peckham, S. E., Grell, G. A., Michalakes, J., Trahan, S., Benjamin, S. G., Alexander, C. R., Dimego, G. J., Wang, W., Schwartz, C. S., Romine, G. S., Liu, Z., Snyder, C., Chen, F., Barlage, M. J., Yu, W., and Duda, M. G. (2017). The Weather Research and Forecasting Model: Overview, System Efforts, and Future Directions. *Bulletin of the American Meteorological Society*, 98(8):1717–1737. 10.1175/BAMS-D-15-00308.1.

Rampanelli, G., Zardi, D., and Rotunno, R. (2004). Mechanisms of Up-Valley Winds. *Journal of The Atmospheric Sciences - J ATMOS SCI*, 61:3097–3111. 10.1175/JAS-3354.1.

Rotach, M. W., Gohm, A., Lang, M. N., Leukauf, D., Stiperski, I., and Wagner, J. S. (2015). On the Vertical Exchange of Heat, Mass, and Momentum Over Complex, Mountainous Terrain. *Frontiers in Earth Science*, 3:76. 10.3389/feart.2015.00076.

Rotach, M. W., Wohlfahrt, G., Hansel, A., Reif, M., Wagner, J., and Gohm, A. (2014). The World is Not Flat: Implications for the Global Carbon Balance. *Bulletin of the American Meteorological Society*, 95(7):1021–1028. 10.1175/BAMS-D-13-00109.1.

Rotach, M. W. and Zardi, D. (2007). On the boundary-layer structure over highly complex terrain: Key findings from MAP. *Quarterly Journal of the Royal Meteorological Society*, 133(625):937–948. 10.1002/qj.71.

Saha, S., Moorthi, S., Pan, H.-L., Wu, X., Wang, J., Nadiga, S., Tripp, P., Kistler, R., Woollen, J., Behringer, D., Liu, H., Stokes, D., Grumbine, R., Gayno, G., Wang, J., Hou, Y.-T., Chuang, H.-Y., Juang, H.-M., Sela, J., and Goldberg, M. (2010). The NCEP climate forecast system reanalysis. *Bulletin of The American Meteorological Society*, 91. 10.1175/2010BAMS3001.1.

Schmidli, J. (2013). Daytime Heat Transfer Processes over Mountainous Terrain. *Journal of the Atmospheric Sciences*, 70(12):4041–4066. 10.1175/JAS-D-13-083.1.

Schmidli, J., Böing, S., and Fuhrer, O. (2018). Accuracy of Simulated Diurnal Valley Winds in the Swiss Alps: Influence of Grid Resolution, Topography Filtering, and Land Surface Datasets. *Atmosphere*, 9(5):196. 10.3390/atmos9050196.

Serafin, S. and Zardi, D. (2010). Daytime Heat Transfer Processes Related to Slope Flows and Turbulent Convection in an Idealized Mountain Valley. *Journal of the Atmospheric Sciences*, 67(11):3739–3756. 10.1175/2010JAS3428.1.

Shea, J., Wagnon, P., Immerzeel, W., Biron, R., Brun, F., and Pellicciotti, F. (2015). A comparative high-altitude meteorological analysis from three catchments in the Nepalese Himalaya. *International Journal of Water Resources Development*, 31(2):174–200. 10.1080/07900627.2015.1020417.

Skamarock, W., Klemp, J., Dudhia, J., Gill, D., Barker, D., Duda, M., Huang, X.-Y., Wang, W., and Powers, J. (2008). A Description of the Advanced Research WRF Version 3. 10.13140/RG.2.1.2310.6645.

Stull, R. (2011). *Meteorology for Scientist and Engineers, 3rd Ed.* Univ. of British Columbia.

Stull, R. B. (1988). *An Introduction to Boundary Layer Meteorology.* Springer Netherlands.

Ueno, K., Toyotsu, K., Bertolani, L., and Tartari, G. (2008). Stepwise Onset of Monsoon Weather Observed in the Nepal Himalaya. *Monthly Weather Review*, 136(7):2507–2522. 10.1175/2007MWR2298.1.

Wagner, J., Gohm, A., and Rotach, M. (2015a). Influence of along-valley terrain heterogeneity on exchange processes over idealized valleys. *Atmospheric Chemistry and Physics*, 15. 10.5194/acp-15-6589-2015.

Wagner, J. S., Gohm, A., and Rotach, M. W. (2014). The Impact of Horizontal Model Grid Resolution on the Boundary Layer Structure over an Idealized Valley. *Monthly Weather Review*, 142(9):3446–3465. 10.1175/MWR-D-14-00002.1.

Wagner, J. S., Gohm, A., and Rotach, M. W. (2015b). The impact of valley geometry on daytime thermally driven flows and vertical transport processes. *Quarterly Journal of the Royal Meteorological Society*, 141(690):1780–1794. 10.1002/qj.2481.

Wang, L., Zhang, Y., Wang, K., Zheng, B., Zhang, Q., and Wei, W. (2016). Application of Weather Research and Forecasting Model with Chemistry (WRF/Chem) over northern China: Sensitivity study, comparative evaluation, and policy implications". *Atmospheric Environment*, 124:337 – 350. https://doi.org/10.1016/j.atmosenv.2014.12.052.

Weigel, A. P. and Rotach, M. W. (2004). Flow structure and turbulence characteristics of the daytime atmosphere in a steep and narrow Alpine valley. *Quarterly Journal of the Royal Meteorological Society*, 130(602):2605–2627. 10.1256/qj.03.214.

Wester, P., Mishra, A., Mukherji, A., and Shrestha, A. (2019). *The Hindu Kush Himalaya Assessment: Mountains, Climate Change, Sustainability and People.* 10.1007/978-3-319-92288-1.

Whiteman, C. (2000). *Mountain Meteorology: Fundamentals and Applications.* Oxford University Press.

Whiteman, C. D. and McKee, T. B. (1982). Breakup of Temperature Inversions in Deep Mountain Valleys: Part II. Thermodynamic Model. *Journal of Applied Meteorology*, 21(3):290–302. 10.1175/1520-0450(1982)021<0290:BOTIID>2.0.CO;2.

Zardi, D. and Whiteman, C. (2013). Diurnal Mountain Wind Systems. *Mountain Weather Research and Forecasting*, pages 35–119. 10.1007/978-94-007-4098-3_2.